

Review

A Review on Pool and Flow Boiling Enhancement Using Nanofluids: Nuclear Reactor Application

Sayantan Mukherjee ¹, Shikha Ebrahim ^{2,*}, Purna Chandra Mishra ¹, Naser Ali ³ and Paritosh Chaudhuri ^{4,5}

- ¹ Thermal Research Laboratory (TRL), School of Mechanical Engineering, Kalinga Institute of Industrial Technology, Bhubaneswar 751024, India; sayantan2210@gmail.com (S.M.); pcmishrafme@kiit.ac.in (P.C.M.)
- ² Mechanical Engineering Department, College of Engineering and Petroleum, Kuwait University, Kuwait City 13060, Kuwait
- ³ Nanotechnology and Advanced Materials Program, Energy and Building Research Center, Kuwait Institute for Scientific Research, Kuwait City 13109, Kuwait; nmali@kisr.edu.kw
- ⁴ Institute for Plasma Research (IPR), Bhat, Gandhinagar 382428, India; paritosh@ipr.res.in
- ⁵ Homi Bhabha National Institute, Anushaktinagar, Mumbai 400094, India
- * Correspondence: shikha.ebrahim@ku.edu.kw

Abstract: Plasma-facing components (PFCs) are used as the barrier to the beam of high heat flux generated due to nuclear fusion. Therefore, efficient cooling of PFCs is required for safety and smooth operation of a fusion reactor. The Hyper Vapotron (HV) is generally used as the heat exchanger to cool down the PFCs during operation. These heat exchangers use pool and flow boiling mechanisms, and hence, their ability is inherently constrained by critical heat flux (CHF). The boiling of nanofluid is very promising as the working fluid in the HV. The efficiency of the HV increases due to the increase in CHF by applying nanofluids. However, the feasibility of nanofluid cooling in fusion reactors needs proper understanding. This paper reviews the recent developments in the utilization of boiling phenomena in nanofluid as a coolant in the HV. Experiments, theoretical studies, significant achievements, and challenges are analyzed and discussed. Finally, important points are indicated for future research.

Keywords: nanofluid; boiling; critical heat flux (CHF); Hyper Vapotron (HV); plasma-facing components (PFCs)



Citation: Mukherjee, S.; Ebrahim, S.; Mishra, P.C.; Ali, N.; Chaudhuri, P. A Review on Pool and Flow Boiling Enhancement Using Nanofluids: Nuclear Reactor Application. *Processes* **2022**, *10*, 177. <https://doi.org/10.3390/pr10010177>

Academic Editor: Blaž Likozar

Received: 13 November 2021

Accepted: 12 January 2022

Published: 17 January 2022

Publisher's Note: MDPI stays neutral with regard to jurisdictional claims in published maps and institutional affiliations.



Copyright: © 2022 by the authors. Licensee MDPI, Basel, Switzerland. This article is an open access article distributed under the terms and conditions of the Creative Commons Attribution (CC BY) license (<https://creativecommons.org/licenses/by/4.0/>).

1. Introduction

Hyper Vapotrons (HVs) are very effective and reliable high-efficiency heat exchangers. A vast development has been carried out in HVs for the last two decades to make them a suitable candidate for high heat flux applications (20–30 MW/m²) in steady state. The HV technology has seen rejuvenation for its possible utilization in plasma-facing components (PFCs) in the International Thermonuclear Experimental Reactor (ITER), Joint European Torus (JET), and the Mega Amp Spherical Tokamak (MAST). The HV uses the Vapotron effect, a very complex inexplicable two-phase phenomenon. However, with the developments in the thermal and flow instruments, it is now easier to trace the characteristics of the Vapotron effect.

The performance of a fusion reactor mainly depends on the performance of the HV and thermal management. Further, the thermal management and performance of the HV depend on the working fluid. In general, water is used as the working fluid in the HV.

Nanofluids are engineered binary mixtures of solid nanoparticles dispersed in base fluids [1]. The solid nanoparticles are metals and their oxides or nonmetals with the particle size typically less than 100 nm. The base fluids are generally water, oils, and other traditional liquids. The concentration of nanoparticles is usually less than 10% by volume. Since the development of nanofluids, they have attracted a large number of research groups with their excellent thermophysical and heat transfer characteristics. The

abundance of the published literature ranges from basic studies containing the formulation and thermophysical properties to the application of nanofluids in convective, boiling, and two-phase flow phenomena [2–10]. These characteristics of nanofluids make them promising for the HV [11–13]. Apart from the original research articles, there are some reviews, that summarized the past investigations and that were directed towards the possible application areas of nanofluids [14–21]. However, to the best of the authors' knowledge, a review on the application of nanofluids in PFCs and HVs is still absent. Therefore, a review on this topic would be suitable to understand the topic better and to encourage the research community to emphasize the least-discussed application areas of nanofluids. Additionally, this review highlights the gap in the literature that needs further investigation.

2. Review Methodology

A literature review is regarded as the major contribution to the research progress. A review earns the adjective “systematic” if it covers clearly formulated questions, recognizes relevant research, estimates the quality of information, and summarizes the verified results in an explicit format [22]. Therefore, a literature review is an assembly of research contributions in the relevant field of study. A systematic review not only analyzes the previous research contributions, but also helps researchers find the answers to the questions they face during their research. The focus of this literature review was on the application of nanofluids in HVs for PFCs. The review was carried out because nanofluids produce heat transfer enhancements that can be utilized to increase the performance of HVs and provide better efficiency and safety with the existing designs. This study adopted the 5-step technique for systematic literature reviews by Khan et al. [22]. The five steps are given as follows.

2.1. Framing Question for the Literature Review

The first phase was to collect the information and examine and analyze the existing studies on the heat transfer in HVs with nanofluids. The existing developments and individual research works were collected. After a thorough analysis, a collection of relevant questions based on the research topic was prepared. The literature review could be initiated by framing such questions. Some of them are presented below:

1. Which individual, research groups or institutions are studying the application of nanofluids in HVs?
2. What are the different experiments carried out in HVs with nanofluids?
3. What are the types of nanomaterials and base fluids being applied?
4. What are the types of preparation methods applied to formulate nanofluids?
5. What are the conditions of the experiments in HVs with nanofluids?
6. What are the parameters measured during experiments with nanofluids in HVs?

2.2. Locating the Appropriate Works

In this phase, some keywords (nanofluid, nanoparticles, nanofluid in nuclear reactors, nanofluid in HV, nanofluid boiling, two-phase flow, heat transfer coefficient, numerical, analytical, and cooling) or their combination connected to the subject and relevant to the objective of the study were identified. Then, a rigorous search was carried out in leading science journals such as Wiley, Elsevier, Taylor and Francis, Springer, etc. The search was also carried out in reputed organizations such as the International Atomic Energy Agency (IAEA), American Society of Mechanical Engineers (ASME), Institute of Physics (IOP), etc. The search was extended to journal indexing or hosting services such as Scopus, Google Scholar, etc.

2.3. Selection and Evaluation of the Quality of the Studies

The Scopus, Science Citation Index (SCI), Science Citation Index Expanded (SCIE), and Emerging Source Citation Index (ESCI) databases were used to collect the relevant data.

The rationale for choosing these databases was that the most influential and high-quality research works are indexed by these databases.

A large amount of reach papers related to the topic of nanofluid are available online. In order to find relevant research works in the particular field, some refinement of the searched results was executed to concentrate only on the important studies. The refinement included inclusion and exclusion criteria to separate relevant and irrelevant data. The inclusion and exclusion criteria are stated below:

I. Inclusion criteria:

1. An article provides applications of nanofluids in PFCs and HVs;
2. An article provides application of nanoparticles and base fluids for PFCs and HV;
3. An article provides boiling or two-phase heat transfer phenomena in nanofluids;
4. An article provides the study of the heat transfer coefficient and critical heat flux in nanofluids;
5. Articles published in the last ten years.

II. Exclusion criteria:

1. Articles not related to PFCs and HV cooling with nanofluids;
2. Articles not presenting boiling or two-phase phenomena with nanofluids;
3. Articles presented in other languages other than English;
4. Short article types such as conference papers, short communications, etc.

Based on the selection criteria, a final list of the particular research articles was prepared. The research outcomes of these selected papers are summarized in this review.

2.4. Briefing the Evidence

A meta-analysis was performed to explore the difference among the selected studies and the integration of their effects. If an overall meta-analysis is not possible due to heterogeneity, then subgroup meta-analysis is applicable. The meta-analysis carried out to frame this review was completely aligned with the criteria listed in Table 1.

Table 1. List of criteria for the meta-analysis.

Grouping	Details
Research interest	Main focus of the study
Research aim	Main objective of the paper
Data type	Quantitative and qualitative categorization of data
Research methodology	Categorization of methods: experimental, numerical, simulation, etc.
Nomenclature of database	Collection of journals presenting nanofluids as reactor coolants and boiling such as pool boiling and flow boiling (two-phase flow)
Year wise sourcing	Year wise journal publications

2.5. Construing the Findings

In order to interpret the findings, the above-mentioned criteria in the previous steps needed to be met. This process assembled the outcomes of the each of the selected papers and provided an organized view that is suitable to understand the rudiments of the studies aiming to provide a detailed outlook to the readers.

3. Statistics of Nanofluid Applications in Fusion Reactors

Based on our survey of the Scopus, Science Citation Index (SCI), Science Citation Index Expanded (SCIE), and Emerging Source Citation Index (ESCI) databases, we found that 0.08% focused on nanofluid applications in PFCs and HVs, 31.13% on boiling heat transfer in nanofluids, and 69.20% on two-phase flow heat transfer in nanofluids including other

potent application areas such as microchannels, refrigeration, industrial heat exchangers, and process technology including fusion reactors. The available documents in the literature focused on the selected categories of papers in the total searched documents are presented by the bar chart in Figure 1.

It is evident from Figure 1 that the research trend in nanofluids is less inclined toward PFCs and HVs in fusion reactors. However, nanofluids and fusion technology are two emerging areas in science and technology.

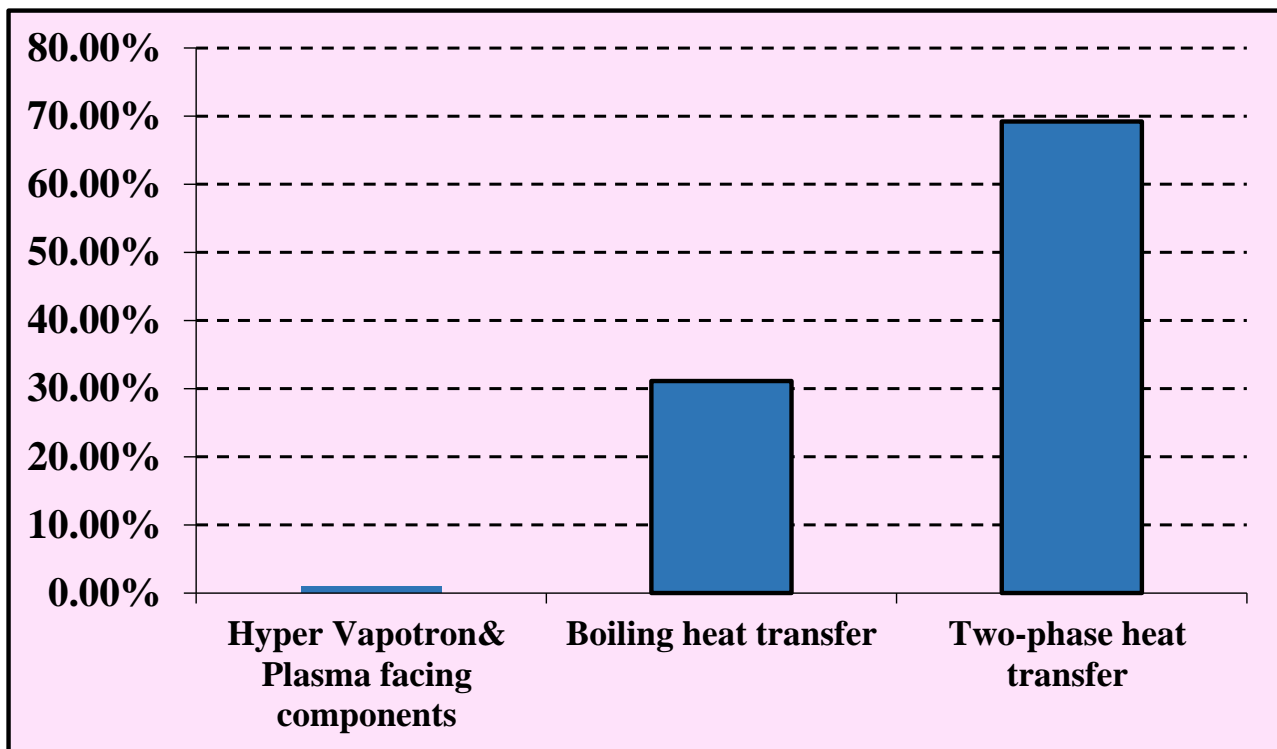
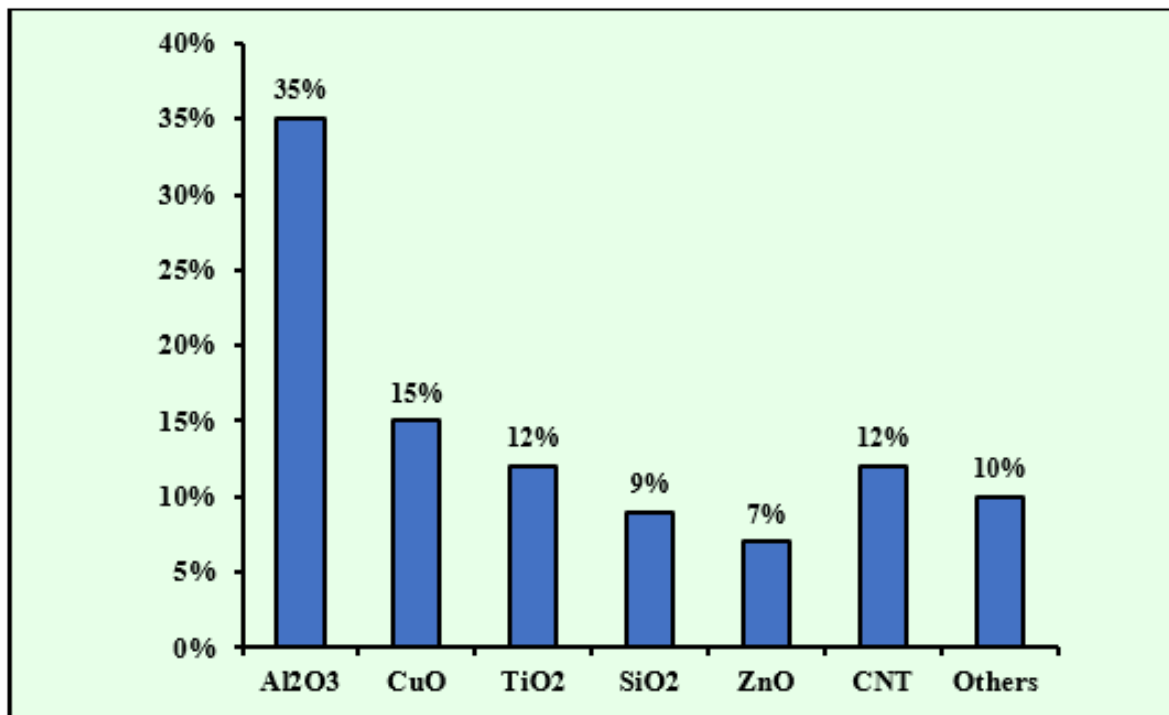


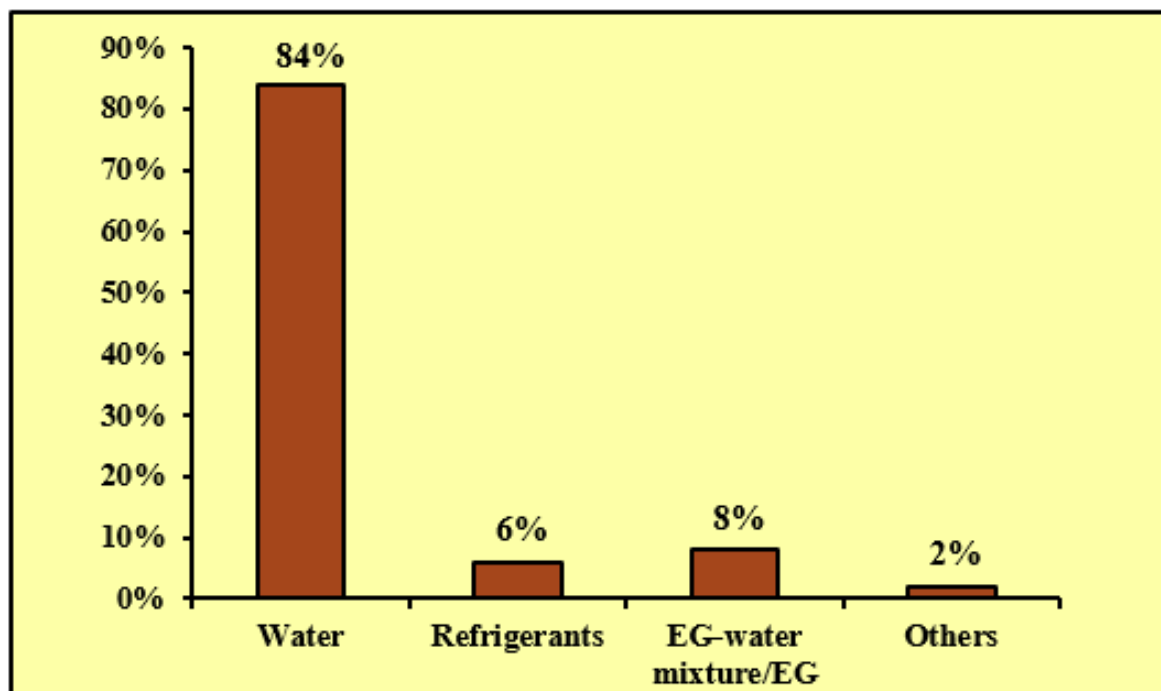
Figure 1. Available literature works published on nuclear fusion, boiling, and two-phase flow with nanofluids.

There are different types of nanoparticles and base fluids applied in the experimental investigations into fusion reactor cooling, boiling, and two-phase heat transfer presented in Figure 2a,b. The illustrations present that Al_2O_3 is the most used type of nanoparticle, followed by CuO, TiO_2 , CNT, SiO_2 , ZnO, ZrO_2 , and Fe_3O_4 , respectively. Water is mostly used as a base fluid followed by an ethylene glycol–water mixture, refrigerant, oils, and others.

Adding nanoparticles to base fluids leads to three different results: (1) augmentations of the heat transfer coefficient (HTC) and critical heat flux (CHF); (2) a decrease in the HTC and CHF; (3) no change. In the present study, we found that 55% of the total searched papers agreed with the first type of result, 37% said deterioration, and the remaining 8% reported inconclusive or no change, as provided in Figure 3.



(a)



(b)

Figure 2. Available literature works on (a) different nanoparticles and (b) different base fluids.

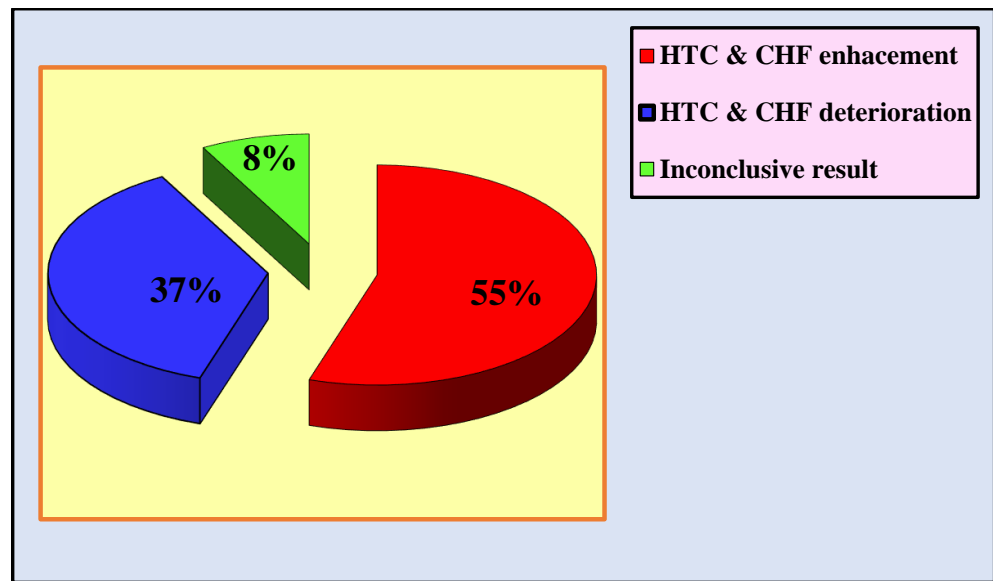


Figure 3. Available literature on investigating the outcomes in boiling heat transfer performance with nanofluids.

4. Progress in Fusion Reactor Cooling Applications with Nanofluids

Progress in PFC cooling with nanofluids has been observed for the last 5–7 y. A review on the available research work is presented in the next section. A list of important studies and their results are presented in Table 2 at the end of this section.

The application of nanofluids is very promising as coolants in PFCs in existing fusion reactors such as the ITER. A 1D simulation of water-based Al_2O_3 fluids under force convection and the subcooled boiling region showed 72% improvement in the CHF even at a very low concentration (0.001% vol. concentration), as demonstrated by Genco and Genco [23]. Such a type of thermal response from nanofluids is suitable to reduce the thermal stress on the cooling tube by increasing the burnout temperature, as shown by Figure 4.

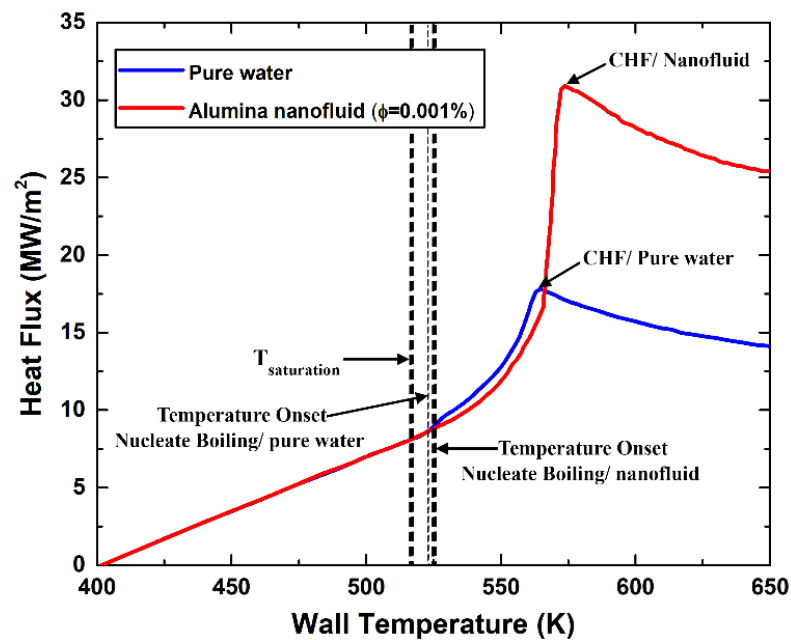


Figure 4. Effect of Al_2O_3 nanoparticle inclusion on the wall temperature and the CHF in PFC cooling.

Sergis et al. [13] used molecular dynamics simulation to analyze the performance of HVs for JET and MAST geometries under the application of a water-based Al_2O_3 nanofluid. The simulation outcome showed a heat transfer enhancement with the nanofluid. They found greater thermal diffusion in the nanofluid compared to the base fluid, and that may increase the bulk thermal conductivity of the nanofluid. The improvement in thermal conductivity may lead to an increase in the heat transfer with the nanofluid. The same research group in later applied a very dilute Al_2O_3 -water nanofluid (0.0001% by volume) in a lab-scale setup of HVs for MAST and JET geometries [11]. A hybrid particle image velocimetry (PIV) was applied to check the flow characteristics of the nanofluid in HVs of the different geometries at three different flow rates of 3 m/s, 6 m/s, and 10 m/s. They reported that the change in the flow characteristics with the addition of nanoparticles in the base fluids was the main reason that enhanced the overall thermal performance of the HV. Moreover, they concluded that the HV technology comprises very complex phenomena and their performance is affected by several parameters. A series of investigations is needed to understand and model those parameters. In addition, they explored the heat transfer performance by single- or two-phase heat transfer mode coupled with the rheology and pumping power requirements for different geometries.

Pan et al. [24] presented an interesting experiment correlated with PFC cooling. They used a triangle-shaped heat sink made of a copper chromium zirconium (CuCrZr) alloy in the HV test. They applied a Al_2O_3 -water nanofluid with a 0.005–0.1% mass concentration under section high heat flux at different flow velocities of 1–3.3 m/s. They reported that the nanofluid at a 0.01% mass fraction showed the best result under different flow velocities and heat fluxes. The enhancement was 22% on average and 30% at most compared to the base fluid. Figure 5 presents the heat transfer performances of the Al_2O_3 nanofluid at selected concentrations and flow velocities. In Figure 5, the heat transfer deteriorated even worse with respect to the water with 0.1% as the increasing nanoparticles in the base fluid caused stability issues, which further caused deposition on the tips of the triangular fins. The deposited nanoparticles greatly enhanced the thermal resistance, causing a sharp deterioration in heat transfer performance. Therefore, the stability of the nanofluid is also important for the heat transfer performance of an HV, as presented by Sergis et al. [13] previously. Apart from this, they found that high heat transfer turned into fully developed subcooled flow boiling. The addition of nanoparticles reduced the bubbles' diameter by thinning the boundary layer. The nanoparticle migration in the dispersed condition produced disturbances in the flow, which greatly enhanced the bubble departure frequency, resulting in the heat transfer performance in the HV.

The compatibility of nanofluids with the PFCs is also an important concern before applying them in practical fusion applications. Nanofluids have shown a serious compatibility issue with the cooling tubes of plasma-facing components. A recent study by Jiang et al. [25] reported that nanofluids are corrosive to the cooling tube materials. The corrosion comes from chemical reaction and mechanical erosion. The CuCrZr alloy had undergone excessive corrosion when a Al_2O_3 -water nanofluid was applied. This may be a reason why nanofluids are still not allowed to be applied in the cooling of PFCs and HVs.

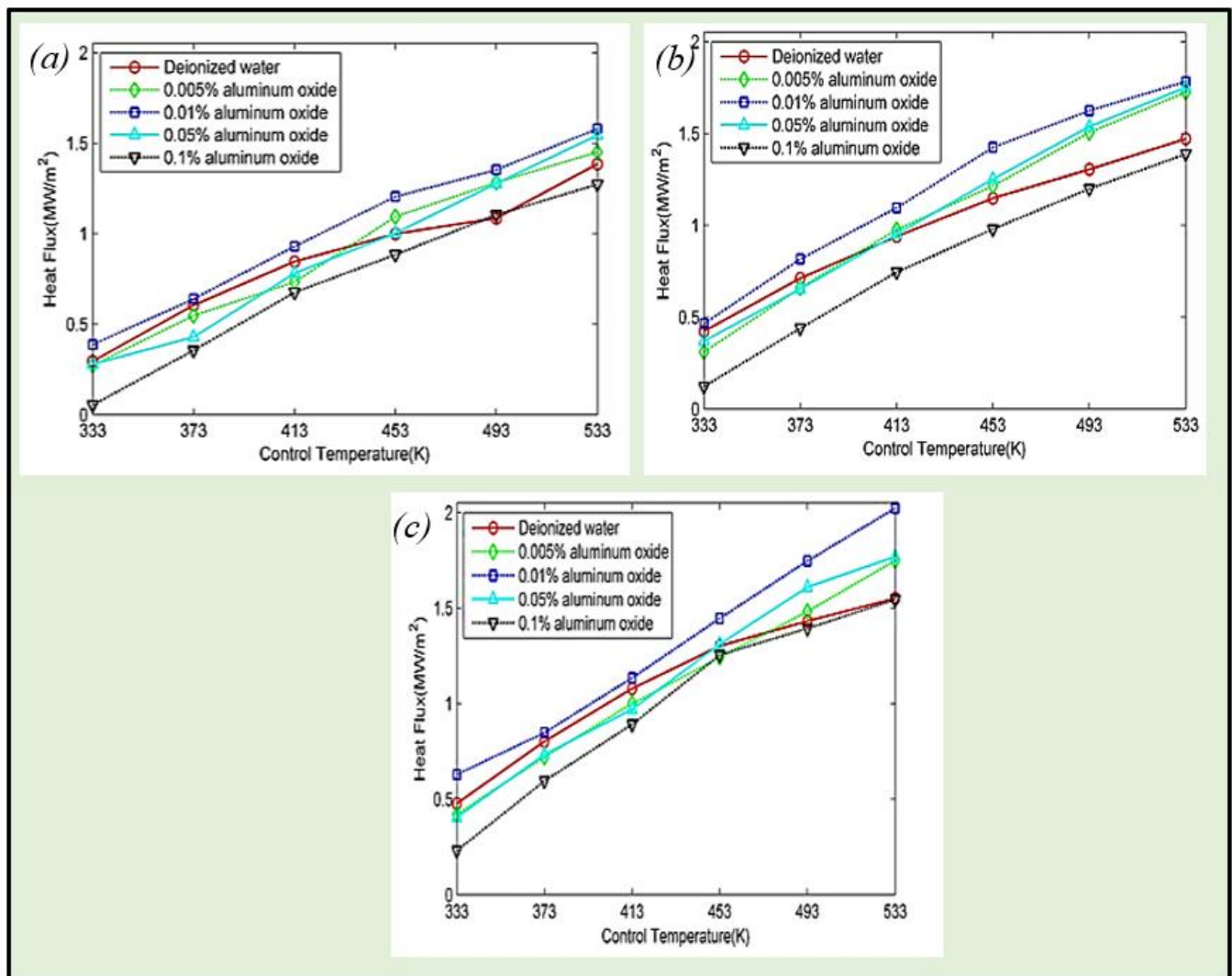


Figure 5. Heat transfer performance with a Al_2O_3 –water nanofluid at different flow velocities (a) at 1 m/s, (b) 2 m/s, and (c) 3.3 m/s. Reproduced with permission from [24]. Elsevier, 2016.

Table 2. Summary of literature works on PFC and HV cooling with nanofluids.

Researchers	Type of Nanofluids; Particle Size; Concentrations (%)	Type of Research	Computational Geometry or Setup	Research Outcome
Sergis et al. [11]	Al_2O_3 –water; 50 nm	Simulation and experiment	Lab-scale HV	Enhancement in heat transfer
Sergis et al. [13]	Al_2O_3 –water, 50 nm; 0.0001%	Experimental and simulation	Lab-scale HV	Enhancement in heat transfer
Genco et al. [23]	Al_2O_3 –water, 0.001%	Simulation	Rectangular channel with swirl inserts for PFC	Enhancement in heat transfer and CHF
Pan et al. [24]	Al_2O_3 –water; 10–20 nm; 0.005–0.01%	Experimental	Lab-scale HV	Enhancement in heat transfer
Jiang et al. [25]	Al_2O_3 –water; 10 nm; 0.01% and 1%	Experimental	A drum with rotatory arrangements	Corrosive effect of nanofluid with increasing concentration

5. Progress in Boiling Heat Transfer with Nanofluids

This section covers the latest studies carried out on the boiling of nanofluids. The boiling phenomenon is generally categorized into two phenomena: (1) pool boiling and (2) flow boiling. All the research in these categories was also subdivided into experimental, analytical, and numerical work.

5.1. Progress in Pool Boiling Heat Transfer with Nanofluids

Experimental Work

You et al. [26] performed pool boiling experiments in a water-based Al_2O_3 nanofluid with concentrations ranging from 0 gm/L to 0.05 gm/L. The nanofluids demonstrated a 200% enhancement in CHF when compared to pure water. Nanofluids are expected to be quintessential as coolants for nuclear reactors. Consequently, pool boiling heat transfers, especially the characteristics of the CHF in nanofluids, have become an area of interest among the various research communities worldwide. A number of research papers have been published. In this section, we review some popular papers from 2011–2020.

Shoghl et al. [27] examined pool boiling experiments of water-based CuO and ZnO nanofluids with or without surfactants using stainless steel vessels with internal rod heaters. They concluded that the nanofluids without surfactant hindered the boiling performance, leading to a smoother heating surface. The addition of surfactant to nanofluids caused an improvement in the boiling heat transfer coefficient. A maximum improvement in the HTC was observed in 0.01 wt.% CuO nanofluids with 0.02 wt.% surfactants. However, the investigators observed a reduction in the boiling HTC due to the development of the bubble film on the heater surface caused by the addition of the surfactants.

Amiri et al. [28] studied pool boiling of water-based CNT nanofluids to develop the impacts of covalent and non-covalent CNT nanofluids on the HTC and CHF. The covalent nanofluid generated more augmentation to the HTC when compared to the non-covalent nanofluid. Additionally, they reported that a decrease in nanoparticle size motivated both the HTC and CHF enhancement.

Huang et al. [29] established nickel wires coated with TiO_2 nanoparticles with the concentration ranging from 0.01–1 wt% using electrical heating in a stainless-steel-made test section. The authors varied the heat flux from 0–1000 KW/m^2 . They reported a notable enhancement in the CHF and a simultaneous deterioration in the HTC with the coated surfaces when compared to the bare surface in pure water. The authors estimated the effect of the wettability and contact angles on the coated and base surfaces. Their experimental observations, provided in Figure 6, demonstrated a decrease in the contact angle with particle loading and rising heat flux. Finally, they concluded that particle inclusion was not the reason for the CHF enhancement, while the modified surface morphology owing to the nanoparticle coating was the prime cause of the CHF enhancement and HTC deterioration by increasing the surface wettability and providing high thermal resistance.

Wen et al. [30] executed an investigation on nucleate boiling of a water-based Al_2O_3 nanofluid using smooth and rough surfaces of brass placed inside a high-temperature Pyrex glass vessel. Their results regarding the enhancement and reduction of boiling heat transfer were completely based on the nanoparticle size distribution, test specimen, and the interactions between them. They concluded that the boiling heat transfer increases with the increase in the roughness during nanofluid boiling.

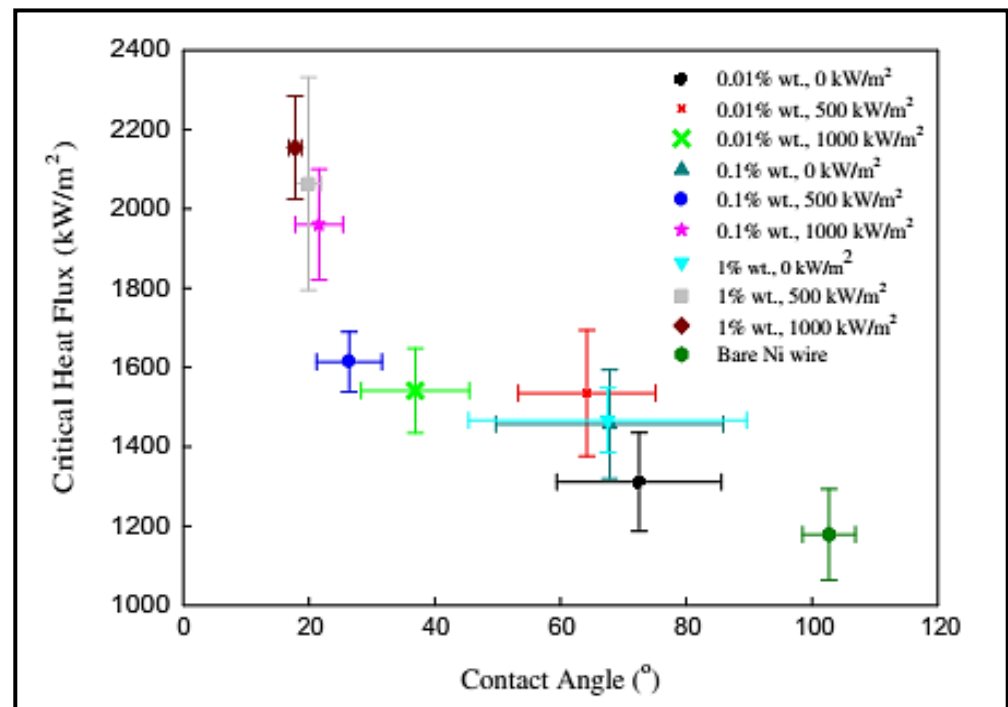


Figure 6. Effect of the contact angle on the CHF with different nano-coated wires. Reproduced with permission from [29]. Elsevier, 2011.

Harish et al. [31] performed pool boiling experiments of electro-stabilized alumina–water nanofluids using smooth and rough heaters arranged horizontally inside a quartz glass tube with a diameter 200 mm. The wettability of the nanofluid with the rough surface was increased with the increase in the particle concentration and decreased with the smooth surface. Furthermore, they opined regarding various surface particle interaction parameters upon which the boiling heat transfer characteristics depend.

Sheikhbahai et al. [32] conducted pool boiling experiments of Fe_3O_4 –EG/water nanofluids using a horizontal thin Ni–Cr wire inside a Pyrex-glass-made round and hollow test pool. The experimental outcome was the decrease in the HTC with increasing nanoparticle concentration. A significant enhancement of 100% in the CHF was noticed for nanofluids with a concentration of 0.1 vol%. These results were mainly due to the alteration of the surface morphology caused by nanoparticle deposition activity during the boiling phenomenon. A significant enhancement in the CHF was noticed with improved wettability and surface roughness due to delayed vapor film blanketing. However, the heat transfer coefficient reduced due to the development of a porous layer with poor thermal conduction on the surface because of the nanoparticle deposition on the heater.

Kole et al. [33] considered the pool boiling characteristics of a ZnO–EG nanofluid utilizing tube-shaped heaters fit inside a stainless-steel-made rectangular pool of 75 mm \times 75 mm \times 200 mm. About a 22% enhancement in the heat transfer coefficient was noticed for nanofluids with a 0.016 vol% concentration. However, the authors were not able to justify their results with valid reasons. The same researchers performed another experiment, and their results demonstrated a 117% enhancement in the maximum CHF for ZnO nanofluids with a concentration of 2.6 vol%. They pronounced that the increased roughness of the test surface was the prime cause of the CHF improvement.

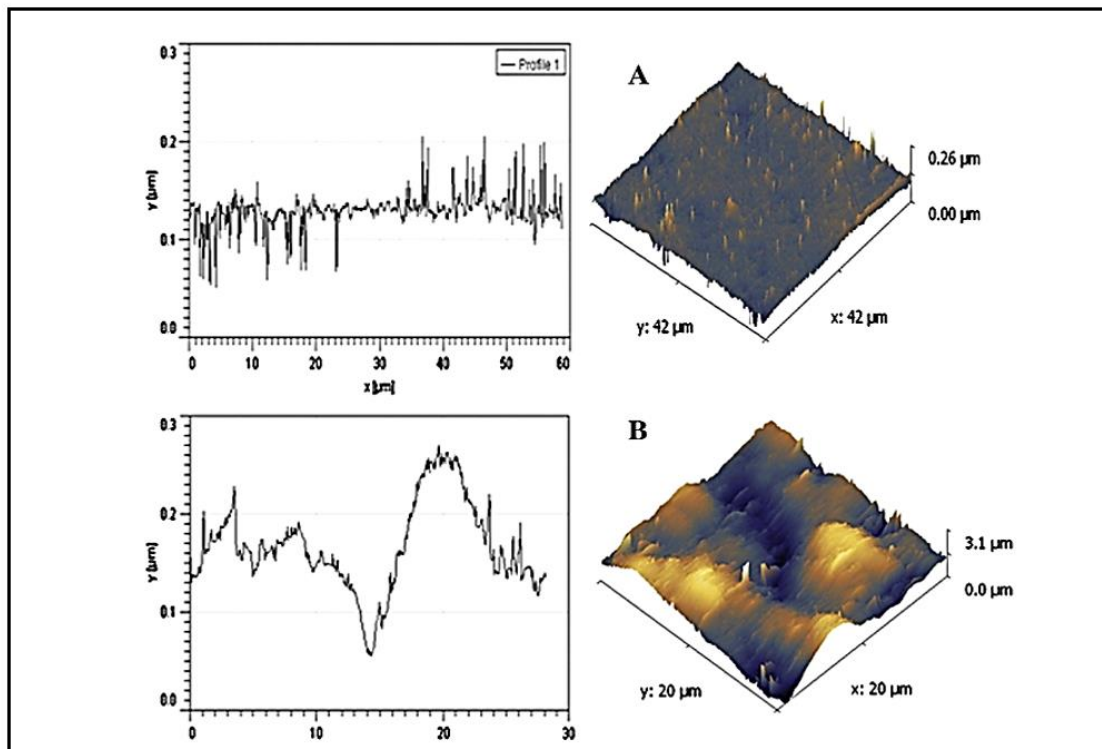
Mourgues et al. [34] carried out pool boiling experiments of water-based ZnO nanofluids at saturated conditions and compared it with the baseline case of deionized water. The test surface used in this study was a disc with a 15 mm diameter. When the test sample was oriented in the vertical position in deionized water, a 19% improvement in the CHF was observed. Similarly, a 54% improvement in the CHF was reported with the nanofluid for both horizontal and vertical orientations of the test sample. A nanoparticle deposition

of ~ 70 μm in thickness on the boiling surface was reported. They noticed a similar CHF for DIW and for the nanofluid with initial nanoparticle deposits on the heating surface. They summarized that the CHF enhancement not happened due to the nanofluid, but likely due to three interdependent parameters, namely wettability, capillary wicking, and roughness.

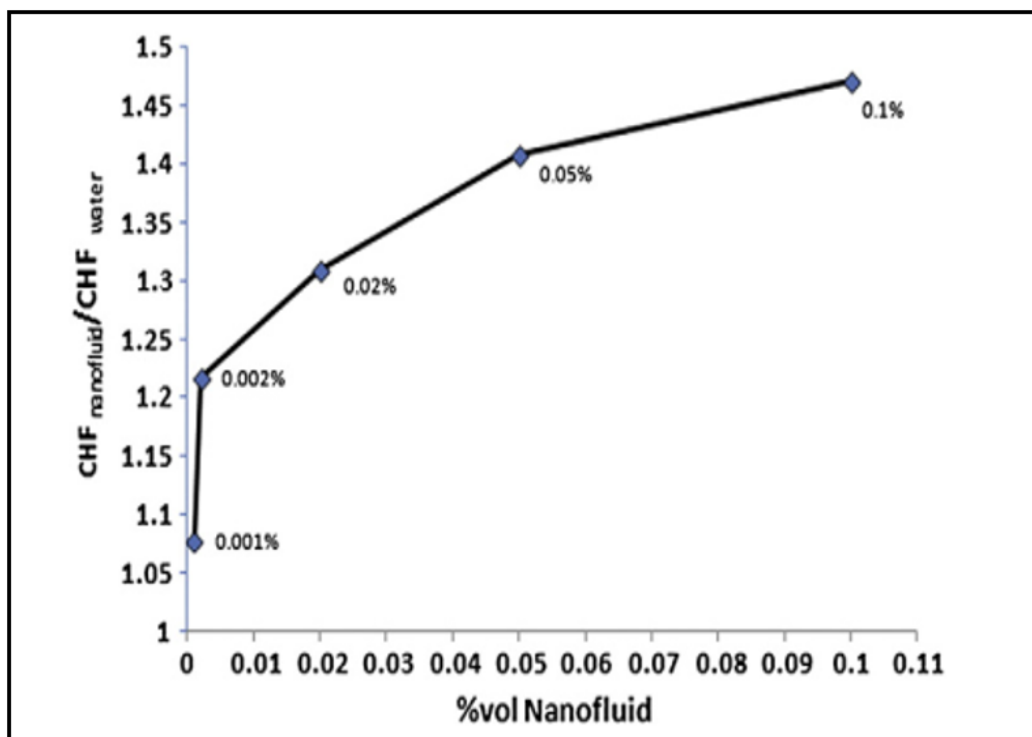
Researchers also tested the pool boiling characteristics of nanofluids in porous metals. The boiling heat transfer increases with the deposition of the nanoparticles on the porous boiling surface. Sarafraz et al. [35] performed an experimental investigation to analyze the nucleate boiling HTC of a Al_2O_3 -EG nanofluid using stainless-steel-made cylinders at different concentrations. The researchers observed a significant increase in the HTC when the heat flux increased in the nanofluids. The nanoparticle deposits on the heating surface increased the fouling resistance and reduced the number of active nucleation sites. Hence, the nanoparticle concentration played a negative role in the enhancement process.

Shahmoradi et al. [36] performed pool boiling experiments of water-based Al_2O_3 nanofluids at concentrations of less than 0.1 vol%. They observed that the deposited nanoparticles developed a porous layer, which improved the wettability, as well as the roughness of the heater surface. As the nanoparticle concentration increased, the surface roughness increased due to the larger size of the particles compared to the surface roughness (AFM images in Figure 7a). The authors reported that the formation of a porous layer on the heater surface further led to an increased thermal resistance and worsened boiling performance. However, the CHF enhanced with particle loading due to improved surface wettability, shown in Figure 7b.

Vafaei et al. [37] examined pool boiling experiments of nanofluids and studied the effects of nanofluid concentration, surface roughness, and heat flux on the heat transfer coefficient. They analyzed the boiling phenomenon of a water-based Al_2O_3 nanofluid on smooth and rough copper surfaces. Figure 8 represents the microscale photographs obtained from SEM analysis and clearly indicates a thin, porous layer of nanoparticle deposited on the rougher heater surface, which altered the cavity size. The size of the nanoparticle deposits increased with the concentration of the nanoparticles in the nanofluid. The nanoparticle deposits on the smooth surface were much bigger than those on rougher surfaces, which led to an improvement in surface roughness and nucleation site density, which in turn improved the HTC using smooth surfaces. The HTC enhancement reduced with the increase in heat flux due to the presence of large cavities, facilitating nucleation at low heat fluxes, and small cavities became active at high heat flux. They also studied the impacts of suspended nanoparticles on the triple-line behavior through the bubble formation method. They concluded that the suspended and deposited nanoparticles played important roles in changing the dynamics of the triple-line, surface wettability, and bubble-forming characteristics.



(a)



(b)

Figure 7. Effect of particle deposition on (a) surface roughness and (b) CHF enhancement. Reproduced with permission from [36]. Elsevier, 2013.

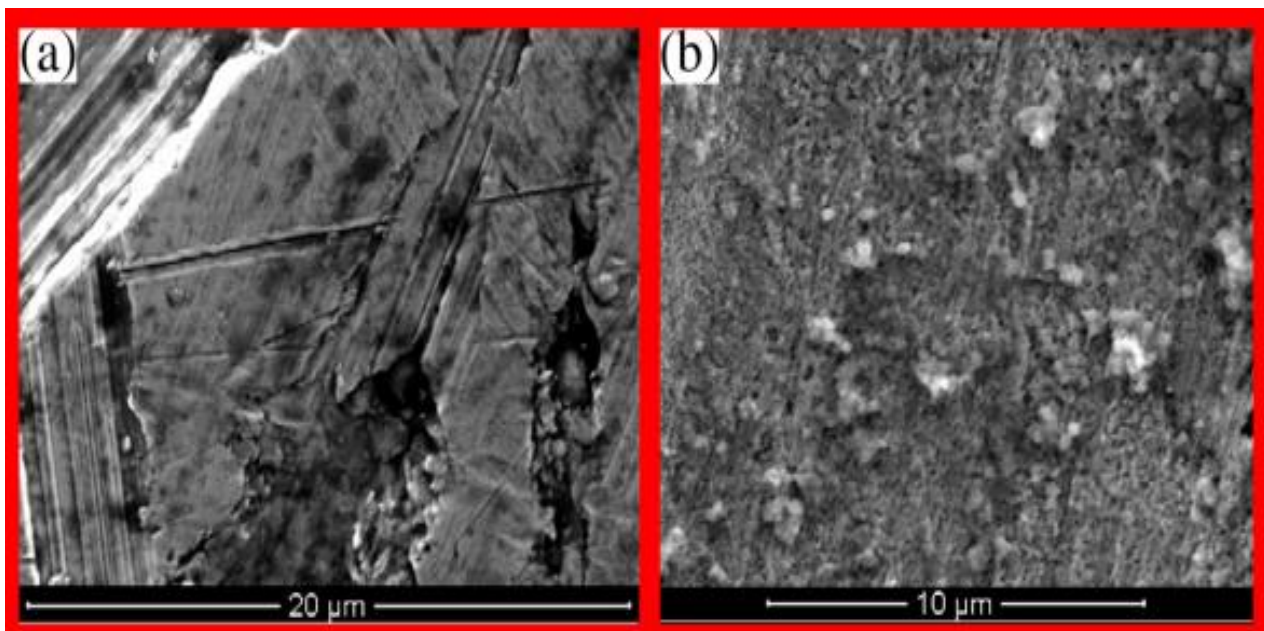


Figure 8. SEM micrographs of a heated rough substrate (a) before and (b) after nanofluid boiling. Reproduced with permission from [37]. Elsevier, 2015.

Cieslinski et al. [38] carried out pool boiling heat transfer experiments of water-based Al_2O_3 and copper nanofluids on a horizontal stainless steel tube heater. The nanofluids were prepared with concentrations ranging from 0.01–1 wt.%. Their results demonstrated a significant enhancement for smooth test specimens. The dispersion of nanoparticles resulted in heat transfer declension due to the nanoparticle-coated surface boiling. The authors reported that with excessive nanoparticles being trapped in the porous matrix, the number of active nucleation sites was reduced, leading to heat transfer degradation during nanofluid boiling. They figured out that the process of blocking the porous structure by nanoparticle deposition was caused by a subsequent pressure drop during the bubble formation inside the porous matrix and the immediate suction of the dispersed nanoparticles into the porous layer just after bubble departure.

Niu et al. [39] experimented with the pool boiling effects of water-based Al_2O_3 and CuO nanofluids on coated porous and polished copper surfaces. A significant enhancement in the HTC was noticed in nanofluids by using the polished and porous surfaces. The bubble development phenomena on both the surfaces were observed using visualization techniques. The visualization results clearly presented a larger bubble departure diameter for the polished surface when compared to the porous surface. In addition to that, the bubble departure diameter was found to be larger when the nanofluids were employed when compared to the base fluids. Therefore, the bubble departure frequency was found to be higher on the porous surface when compared to the polished surface for both the nanofluids.

Kamatchi et al. [40] investigated the pool boiling heat transfer characteristics of water-based rGO (reduced graphene oxide) nanofluids on an electrically heated thin Ni–Cr wire under atmospheric pressure. A significant enhancement of 145% to 245% in the CHF was observed by employing dispersed rGO nanoparticles. The authors confirmed that rGO deposits developed a layer on the surface that increased the pore volume to hold the liquid and to facilitate the capillary-induced flow towards the dry area, below the bubble departure area, which could effectively delay the occurrence of local dryout. They also confirmed an increase in the thickness of the layer with the increase in the concentration of the nanoparticles. They studied the improvement in the CHF based on surface wettability, surface roughness, and porous layer thickness. They concluded that the liquid microlayer

dryout theory model was aligned with the mechanisms involved in the CHF improvement of the Ni–Cr wire with rGO deposits.

Sarafraz et al. [41] studied the pool boiling heat transfer characteristics of aqueous CNT and functionalized carbon nanotube (FCNT) nanofluids. The results demonstrated significant enhancements in the CHF and HTC when FCNT nanofluids were employed when compared to CNT nanofluids. The nanoparticle fouling developed on the heater surface, reduced the capillary wicking, and increased the thermal resistance, resulting in a decrease in the HTC and a slight improvement in the CHF. They concluded that FCNT nanofluids depicted a substantial improvement in the CHF and HTC when compared to CNT nanofluids. This is because the FCNT deposits did not significantly change the surface roughness and provided improved surface wettability with lowered contact angles, which absorbed more nanoparticles to the porous layer, leading to a strong improvement in the CHF.

Sayahiet et al. [42] examined the pool boiling of nanofluids to predict the superior coolant among water-based γ -Al₂O₃, SiO₂, and ZnO nanofluids each of a 0.03% mass concentration under a 100 kPa saturation pressure, varying the heat flux from 7–330 kW/m². Sodium dodecyl sulfate (SDS) was used as the surfactant at a concentration of 0.01 wt%. The γ -Al₂O₃ nanofluids demonstrated an enhancement in the HTC, but a deterioration in the enhancement was noticed with the addition of SDS. This was mainly due to the increase in the viscosity and the reduction in the surface tension of the nanofluid, with the addition of SDS surfactants. The SiO₂–water nanofluids weakened the HTC enhancement, and the ZnO–water nanofluids presented the best performance among the three, in the presence of SDS.

Manetti et al. [43] executed pool boiling experiments of water-based Al₂O₃ nanofluids with vol. fractions of 0.0007% and 0.007% over a cylindrical copper surface of two different roughnesses. They reported a 15% enhancement in the HTC with the rough surface and 75% with the smooth surface. They also concluded that the change of the surface roughness due to particle deposition was a key parameter in the pool boiling of nanofluids.

Very recently, Sayantan et al. [44] performed pool boiling experiments of Al₂O₃–water and TiO₂–water nanofluids at different concentrations ranging from 0.01–1% wt. fractions. The heat flux was varied from 2.08–4.69 MW/mm². They reported significant improvements in boiling performance up to 0.1% with increasing heat flux. However, it decreased beyond that concentration. The surface wettability of the boiling surface increased with the application of nanofluids, which led to an improvement in the boiling heat transfer with particle addition, as shown in Figure 9. However, the decrease in surface roughness from the rapid deposition of the nanoparticles at higher concentrations led to a decrease in the boiling performance of the nanofluids.

Some important experimental work regarding pool boiling in nanofluids was discussed above. A summary of these research works is listed in Table 3.

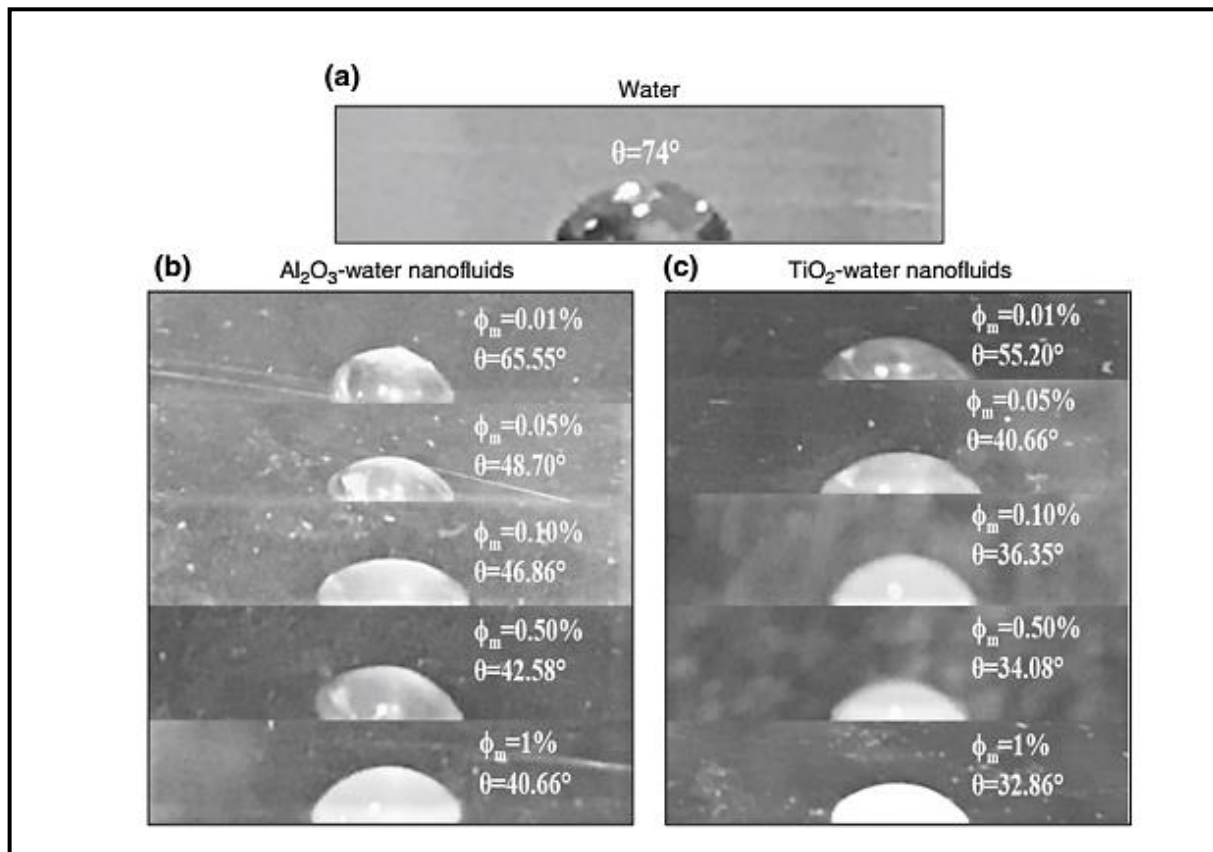


Figure 9. Surface wettability study of nanofluids by Sayantan et al. [44]. Reproduced with permission from [44]. Springer Nature, 2020.

Table 3. Summary of pool boiling experiment on nanofluids.

References	Heating Surface	Nanofluids; Particle Size; Concentration	Surface Analysis	HTC or CHF Enhancement/Deterioration
You et al. [26]	Cu plate	Al_2O_3 -water, SiO_2 -water	-	200% enhancement in CHF
Shoghl et al. [27]	SS cylinder ($\text{Ø}10.67 \times 99.1 \text{ mm}^2$)	CuO -water and ZnO -water; 0.01–0.02%	SEM and AFM	HTC enhancement at low concentration and deterioration at high concentration
Amiri et al. [28]	Heater ($\text{Ø}15 \times 75 \text{ mm}$)	CNT-water, $<\text{Ø}60 \text{ nm} \times 15 \text{ mm}$; 0.01–0.1 wt.%		HTC enhancement for covalent nanofluid; deterioration for non-covalent nanofluid; 274.2% enhancement in CHF
Huang et al. [29]	Nickel wire ($\text{Ø}0.3 \times 50 \text{ mm}$)	TiO_2 -water; 110–220 nm; 0.01 to 1 wt.%	SEM	Deterioration in HTC; 82.7% enhancement in CHF
Wen et al. [30]	Cu plate ($20 \times 20 \text{ mm}^2$) with rough and smooth surface	α - Al_2O_3 -water; 20–150 nm; 0.001–0.1 vol.%	SEM and AFM	Enhancement in HTC for smooth surface; HTC unchanged for rough surface; no data for CHF for both studies
Harish et al. [31]	An aluminum disk with smooth and rough surface	Al_2O_3 -water; $<50 \text{ nm}$; 0.5–2 vol.%	AFM	HTC enhanced only on rough surface; no report on CHF

Table 3. Cont.

References	Heating Surface	Nanofluids; Particle Size; Concentration	Surface Analysis	HTC or CHF Enhancement/Deterioration
Sheikhbahai et al. [32]	Ni–Cr wire	Fe ₃ O ₄ –EG–water; <50 nm; 0.01–0.1 vol.%	SEM	HTC deteriorated; no report on CHF
Kole et al. [33]	Cu block of 15 mm diameter	ZnO–EG; <50; 0.5–3.75 vol.%	Profilometer	22% enhancement in HTC with 1.6 vol.%; no data for CHF
Mourgues et al. [34]	SS disk of 15 mm diameter	ZnO–water; 0.01 vol.%	Photograph	HTC enhancement; 54% enhancement in CHF
Sarafraz et al. [35]	Copper cylinder and honeycomb porous plate installed on it (Ø10, Ø30, Ø50)	TiO ₂ –water; 21 nm; 0.0011 vol.%	-	HTC deteriorated; 220% enhancement in CHF
Shahmoradi et al. [36]	Copper block of 38 mm diameter	Al ₂ O ₃ –water; 40 nm, 0.001–0.1 vol.%	AFM	40% deterioration in HTC; 47% enhancement in CHF
Vafaei et al. [37]	Copper substrate (20 × 20 mm ²)	Al ₂ O ₃ –water; 0.001–0.1 vol.%	AFM and SEM	Enhancement in HTC
Cieslinski et al. [38]	SS tube of outer dia 10 mm, 0.6 mm wall thickness	Al ₂ O ₃ –water; 5–250 nm; 0.01–1 wt.%, Cu–water; 7–257 nm; 0.01–1 wt%	TEM	HTC enhanced for smooth tubes; deteriorated for coated tube
Niu et al. [39]	Copper heating block	Al ₂ O ₃ –water; 20 nm; 0.1 vol% CuO–water; 20 nm; 0.1 vol%	SEM	Enhancement in HTC
Kamatchi et al. [40]	Ni–Cr wire	rGO–water; 0.01–0.3 g/L	XRD, SEM, and FT-IR	No report for HTC; 145–245% enhancement in CHF
Sarafraz et al. [41]	Discoid copper heater of surface area 78 mm ²	CNT–water and FCNT–water; 10–20 nm diameter 1.5–2 µm length; 0.1–0.3 wt.%	TEM, XRD, and SEM	HTC deteriorated; CHF enhanced
Sayahi et al. [42]	Cylindrical boiling vessel	γ-Al ₂ O ₃ –water; 10 nm; 0.03 wt.%, SiO ₂ –water; 10–20 nm; 0.03 wt% ZnO–water with SDS; 0.03 wt%	TEM, AFM	56% enhancement in HTC with γ-Al ₂ O ₃ –water nanofluids; deterioration in HTC with SiO ₂ –water nanofluids; 60% enhancement in HTC with ZnO–water with SDS
Manetti et al. [43]	Cylindrical copper block (Ø20 × 60 mm ²)	Al ₂ O ₃ –water; 10 nm; 0.0007 vol.% and 0.007 vol.%	Roughness profiler	75% enhancement in HTC with smooth surface; 15% enhancement in HTC for rough surface
Sayantana et al. [44]	Rectangular Steel vessel (330 mm × 300 mm × 420 mm)	Al ₂ O ₃ –water, TiO ₂ –water; 0.01–1 wt.%	Surface roughness profiler	HTC and CHF enhanced for lower concentrations, but decreased at higher concentrations
Salimpour et al. [45]	Cylindrical copper block (Ø45 × 100 mm ²)	Fe ₃ O ₄ –water; 0.1% and 0.5% vol. fraction	AFM	With rough surface, HTC reduced at low heat flux, but increased at high heat flux; with smooth surface, HTC increased at low heat flux and remained unchanged at high heat flux
Li et al. [46]	Copper heating rod (100 mm long, 10–20 mm)	CuO–water;	-	20–22% enhancement in HTC
Kouloulis et al. [47]	Ni–Cr wire	Al ₂ O ₃ –water; 0.0012 and 0.0024 vol.%	SEM	-
Etedali et al. [48]	Copper block (40 mm wide and 90 mm long)	Si–water with CTAB, Ps20 and SLS; 50 nm, 0.01–1 vol.%	Surface profiler	HTC significantly enhanced with surfactant addition

5.2. Analytical and Numerical Work

Apart from experimental works, few analytical studies were also carried out to predict the pool boiling performance of various nanofluids. The following portion summaries those works. A list of such works was also prepared and is presented in Table 4.

Li et al. [49] used rectangular-shaped cells in a 2D computational domain to carry out an analytical study regarding nucleate boiling heat transfer. The experimental results obtained were significantly aligned with the numerical two-fluid model. The developed correlation verified the heat transfer, nucleation site density, and bubble departure diameter during boiling caused by nanoparticle Brownian movement. Simulation-based outcomes verified that the accuracy of nucleate boiling in nanofluids was enhanced with nucleate site density and nanoparticle Brownian movement due to the change in surface morphology. They finally proposed a correlation for the bubble departure diameter.

$$d_b = C_b \frac{2 + 3 \cos \theta - \cos^3 \theta}{4} \sqrt{\frac{\sigma}{g(\rho_l - \rho_g)}} \exp\left(-\frac{\Delta T_{sub}}{45}\right) \quad (1)$$

Kamel et al. [50] numerically investigated the pool boiling characteristics of pure water and water-based silica nanofluids inside a rectangular boiling chamber. They utilized a two-phase Eulerian–Eulerian model to determine the boiling curve and interaction between two phases. The heat flux partitioning model was used in their study. Their simulation incorporated surface roughness and wettability. The simulation result demonstrated that the effect of the vapor fraction in pure water was more significant than to that in the nanofluid at a certain super heat temperature and that the phenomenon was caused by the nanoparticle deposition on the boiling surface. The pool boiling HTC was estimated as lower than the base fluid. Moreover, they also described the critical heat flux as a significant parameter in pool boiling heat transfer. Later, they proposed a correlation for the bubble waiting time.

$$N_a = \frac{512}{\gamma} Pr_l^{1.63} \left[14.5 - 4.5 \left(\frac{PRa}{\sigma} \right) + 0.4 \left(\frac{PRa}{\sigma} \right)^2 \right] \beta^{-0.4} \zeta \left(\frac{Ra}{d_p} \right)^{0.4} \Delta T_{sup}^3 \quad (2)$$

$$\zeta \left(\frac{Ra}{d_p} \right) = \begin{cases} 0.275 \left(\frac{Ra}{d_p} \right)^{-1.2} & \left(\frac{Ra}{d_p} \right) \leq 1 \\ 0.275 + 0.7911 \left(\frac{Ra}{d_p} \right)^{0.68} & \left(\frac{Ra}{d_p} \right) > 1 \end{cases} \quad (3)$$

Salehi et al. [51] executed a numerical study regarding the pool boiling of water-based silica nanofluids at a 0.01% vol. fraction using a two-phase Eulerian multiphase scheme. They also used a heat flux partitioning approach to predict the bubble parameters. The results demonstrated the particle deposition on the boiling surface as a significant parameter in controlling the boiling of the nanofluid. The boiling HTC was found to deteriorate with nanoparticle addition. This may indicate that the particle deposition effect hinders the heat transfer by enhancing the thermal resistance between the heating surface and test fluid.

Balcilar et al. [52] applied various artificial neural network methodologies for predicting boiling heat transfer in a TiO₂ nanofluid with a 0.0001–0.01% vol. fraction. They also reported that the artificial neural methods yielded better results in predicting the heat flux and the boiling HTC than the existing empirical models and correlations. The boiling HTC was found to be dependent on the liquid dynamic viscosity, wall super heat, nanoparticle concentration, liquid density, and roughness of the heating surface.

Very recently, Ganapathy et al. [53] proposed a semi-analytical approach to determine heat flux and nucleation site density for boiling in a nanofluid. They introduced two new parameters, which were surface particle interaction and wettability, in the development of the model. Their result showed a 30% decrement in boiling heat transfer with the nanofluid.

However, they achieved a 67% enhancement in heat transfer in base fluid boiling on the nanoparticle-coated surface. The new model is presented below.

$$q_{Total} = 0.25 \left(\frac{\gamma \phi \sqrt{\pi}}{10} B^2 A r^{0.27} J a \alpha_l^{1.5} t_g^{0.5} \rho_l \lambda N_a x \right) + 0.75 \left(2 \sqrt{\frac{k_l \rho_l C_{p,l}}{\pi t_w}} K N_a \frac{\pi D_{b,d}^2}{4} \Delta T x \right) + \left(0.14 \frac{k_l}{L} G r . P r^{\frac{1}{3}} A_{nc} \Delta T \right) \quad (4)$$

$$N_{a,nf} = 218.8 \frac{1}{\gamma} P r^3 \Delta T^3 \left[\left(14.5 - 4.5 \left(\frac{R_a P}{\sigma} \right) + 0.4 \left(\frac{R_a P}{\sigma} \right)^2 \right) \times \left(\frac{1 - \cos \theta}{1 - \cos \theta^*} \right)^3 \left(\frac{R_a}{D_p} \right)^{-0.5} \right]^{-0.4} \quad (5)$$

The complexity of pool boiling heat transfer can be easily understood by the Soret effect or thermo-diffusion phenomena in nanofluids. Gobinath et al. [54] investigated the pool boiling of a water-based Al₂O₃ nanofluid with different heater temperatures ranging from 50–90 °C. They used ANSYS Fluent to simulate the experiment with the 2D-steady-pressure-based implicit solver with the Gauss–Seidel iterative procedure for solving mathematical models. The SIMPLE algorithm was used for pressure correction in the model. The thermophoretic parameters such as the Peclet number and time-scale equation were applied to simulate the particle movement due to nanoscale heat transfer. The result displayed that the velocity of the nanoparticles had a diminishing effect near the heater surface. The combined effect of the Peclet number and time-scale diffusion fortified the thermo-diffusion and advection process in the heat transfer process.

Table 4. Summary of analytical and numerical works on pool boiling in nanofluids.

Researchers	Type of Nanofluids	Modeling and Correlations	Remarks	Research Outcome
Li et al. [49]	Si–water	Numerical modeling $d_b = C_b \frac{2 + 3 \cos \theta - \cos^3 \theta}{4} \sqrt{\frac{\sigma}{g(\rho_l - \rho_g)}} \exp\left(-\frac{\Delta T_{sub}}{45}\right)$	Influence of Brownian motion is taken into the model development. Numerical two-fluid model is considered. Bubble departure diameter is presented.	Brownian motion is important in boiling heat transfer. A decrease in the HTC observed with nanofluids. Accurate prediction of pool boiling heat transfer in nanofluids with the proposed model. Wettability, surface characteristics, and bubble diameters are important to predict the boiling in nanofluids.
Kamel et al. [50]		Numerical simulation and analysis $N_a = \frac{512}{\gamma} P r_l^{1.63} \left[14.5 - 4.5 \left(\frac{P R_a}{\sigma} \right) + 0.4 \left(\frac{P R_a}{\sigma} \right)^2 \right] \beta^{-0.4} \zeta \left(\frac{R_a}{d_p} \right)^{0.4} \Delta T_{sup}^3$ $\zeta \left(\frac{R_a}{d_p} \right) = \begin{cases} 0.275 \left(\frac{R_a}{d_p} \right)^{-1.2} & \left(\frac{R_a}{d_p} \right) \leq 1 \\ 0.275 + 0.7911 \left(\frac{R_a}{d_p} \right)^{0.68} & \left(\frac{R_a}{d_p} \right) > 1 \end{cases}$	Two-phase Eulerian–Eulerian approach and phase interactions are considered. Wettability and surface roughness are incorporated.	Effect of the vapor fraction in pure water is more significant. Quenching heat flux plays a dominant role in pool boiling heat transfer.
Salehi et al. [51]	Si–water, 0.01%	Numerical simulation and analysis	Two-phase Eulerian multiphase scheme with the heat flux partitioning model is applied to predict the bubble parameters.	Particle deposition on the boiling surface plays a key role in controlling the boiling of the nanofluid. Deposition effect hinders the heat transfer by enhancing the thermal resistance between the heating surface and test fluid
Balcilar et al. [52]	TiO ₂ –water	ANN-based modeling	The artificial neural methods yield better results on predicting the heat flux and the boiling HTC than the existing empirical models and correlations.	Boiling HTC was found dependent on the liquid dynamic viscosity, wall super heat, nanoparticle concentration, liquid density, and roughness of the heating surface.

Table 4. Cont.

Researchers	Type of Nanofluids	Modeling and Correlations	Remarks	Research Outcome
Ganapathy et al. [53]	Al ₂ O ₃ -water	$q_{Total} = 0.25 \left(\frac{\gamma \phi \sqrt{\pi}}{10} B^2 Ar^{0.27} Ja \alpha_l^{1.5} \mu_g^{0.5} \rho_l \lambda N_a x \right) + 0.75 \left(2 \sqrt{\frac{k_l \rho_l C_{p,l}}{\pi t_w}} K N_a \frac{\pi D_{b,d}^2}{4} \Delta T x \right) + \left(0.14 \frac{k_l}{L} Gr \cdot Pr^{\frac{1}{3}} A_{nc} \Delta T \right)$ $N_{a,nf} = 218.8 \frac{1}{7} Pr^3 \Delta T^3 \left[\left(14.5 - 4.5 \left(\frac{R_a P}{\sigma} \right) + 0.4 \left(\frac{R_a P}{\sigma} \right)^2 \right) \times \left(\frac{1 - \cos \theta}{1 - \cos \theta^*} \right)^3 \left(\frac{R_a}{D_p} \right)^{-0.5} \right]^{-0.4}$	Surface particle interaction, wettability parameter.	67% enhancement in heat transfer in base fluid boiling on the nanoparticle-coated surface.
Gobinath et al. [54]	Al ₂ O ₃ -water	ANSYS simulation	2D steady-pressure-based implicit solver with Gauss–Seidel iterative procedure for solving the mathematical model.	The velocity of nanoparticles has a diminishing effect near the heater surface. The combined effect of the Peclet number and time-scale diffusion fortify the thermo-diffusion and advection process in the heat transfer process

6. Progress in Flow Boiling Heat Transfer with Nanofluids

6.1. Experimental Work

This section describes a brief review of the important experimental research conducted on flow boiling in recent years.

Sarafraz et al. [55] examined flow boiling of MgO (50 nm) nanoparticles in Therminol 66 nanofluid at concentrations ranging from 0.1–0.3 wt.%. The experimental facility used for the study is presented in Figure 10. The test loop included a circulation loop, a testing chamber, and measuring instruments. The results presented a decrease in the HTC with time, and this was due to the formation of a porous layer on the surface through nanoparticle deposits. Additionally, the HTC increased when compared to Therminol 66. The best enhancement was found when a 0.1% mass concentration was used. They concluded that MgO nanofluids exhibited the best performance with a dilute concentration for boiling applications.

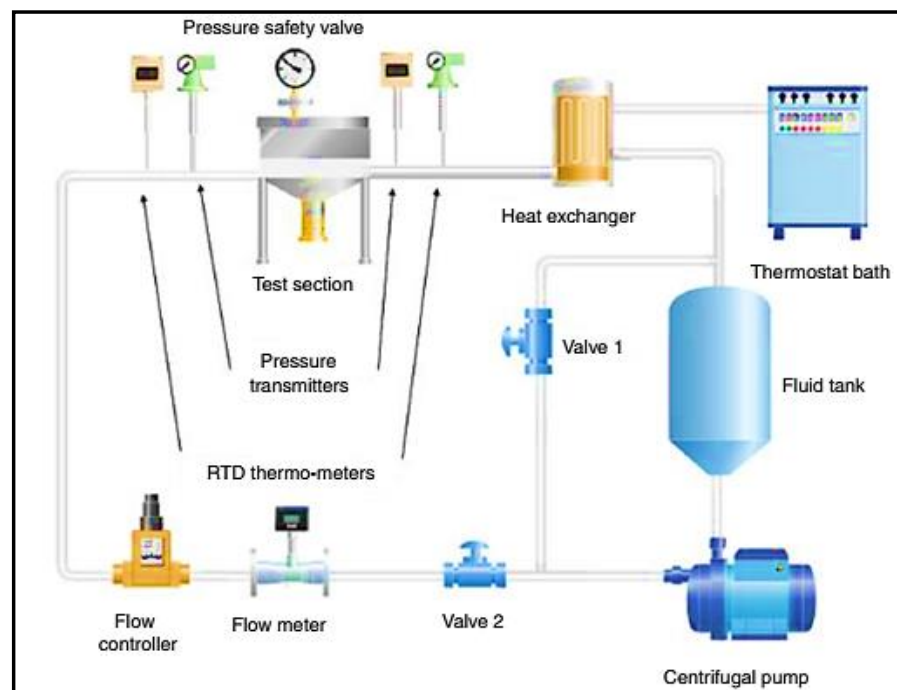


Figure 10. Schematic of the experimental flow boiling test rig used by Sarafraz et al. [55]. Reproduced with permission from [55]. Elsevier, 2018.

Karimzadehkhoei et al. [56] inspected the subcooled flow boiling of water-based γ - Al_2O_3 nanofluids inside horizontally placed stainless steel microtubes. The authors focused on the impacts of the surface morphology and nanoparticle deposits. Concentrations ranging from 0.05–1.5 wt.% and mass fluxes of 1200 $\text{kg}/\text{m}^2 \text{ s}$ and 3400 $\text{kg}/\text{m}^2 \text{ s}$ were applied to investigate the boiling performance of the nanofluid. The enhancement in the HTC of the nanofluid decreased with particle loading, as shown in Figure 11. Besides this, the HTC with lower concentrations demonstrated similar results to that of distilled water. They pointed out that the accumulation of nanoparticles was the primary reason for the degradation of the HTC during the study.

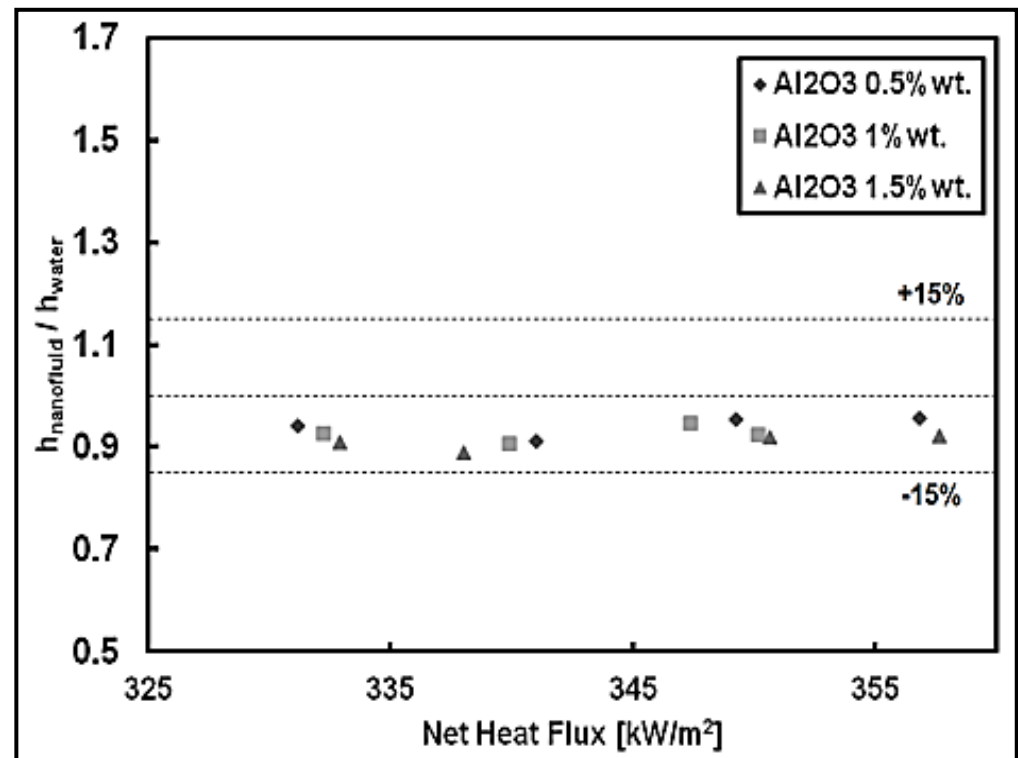


Figure 11. Decrease in HTC enhancement against net heat flux at increasing particle loading. Reproduced with permission from [56]. Elsevier, 2017.

Hashemi et al. [57] investigated the flow boiling performance of a multi-walled carbon nanotube (MWCNT)–water nanofluid in a horizontal stainless steel tube under atmospheric pressure. They applied gum Arabic (GA) as a stabilizer, and its stability was estimated by zeta-potential analysis. Their results demonstrated an enhanced CHF in comparison to pure water. Furthermore, the HTC of the nanofluid was more significant than that of water. Choi et al. [58] demonstrated CHF enhancement in subcooled flow boiling of water-based Fe_3O_4 nanofluids in a vertical test section. The experiment was carried out with a mass flux up to 5000 $\text{kg}/\text{m}^2 \text{ s}$ and inlet subcooled temperatures in the range of 40–80 °C. Their results demonstrated a maximum enhancement of 40% in the CHF with the increase in mass flux. Figure 12 demonstrates the CHF enhancements with the mass flux for different subcooled inlet temperatures carried out in their study. Such an enhancement was attributed to the increasing surface wettability with a significant reduction in the contact angle from 82° to 30°, resulting from the deposits of the nanoparticles on the surface.

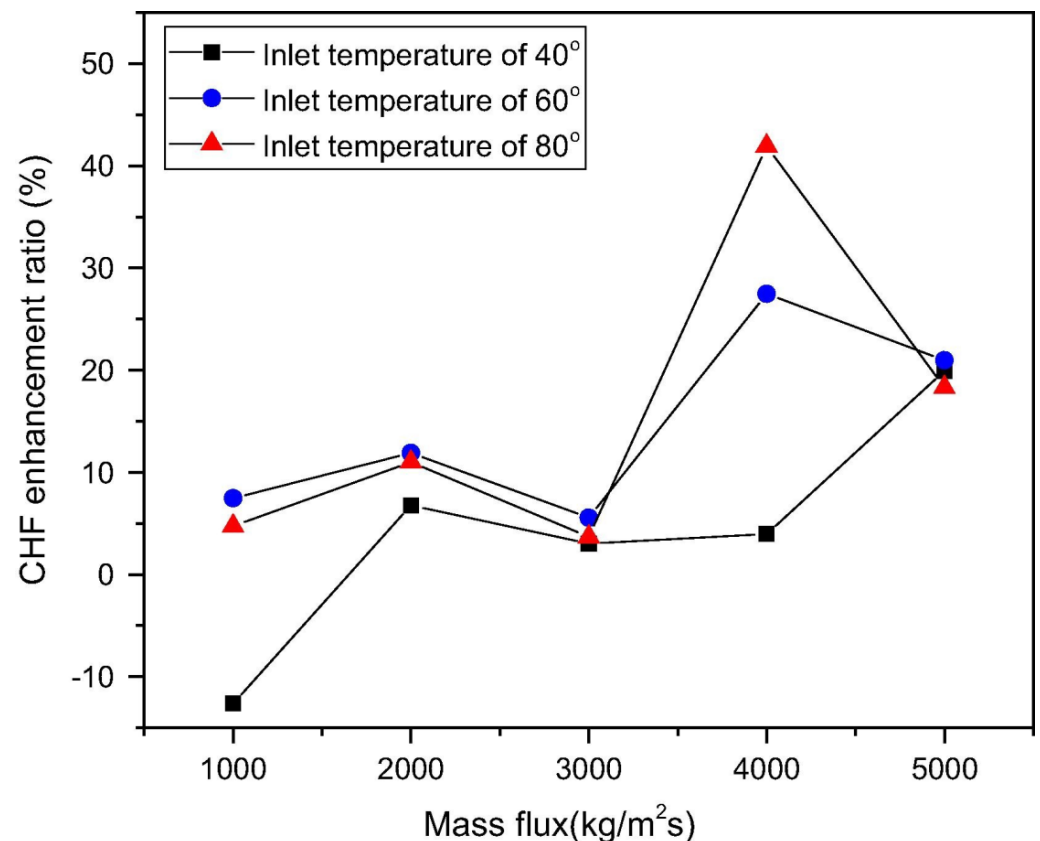


Figure 12. CHF enhancement in a Fe_3O_4 -water nanofluid against mass flux at different inlet temperature. Reproduced with permission from [58]. Elsevier, 2017.

Rajabnia et al. [59] investigated the subcooled flow boiling of water-based TiO_2 (20 nm) nanofluids at three different volume concentrations (i.e., 0.01%, 0.1%, and 5%) inside a horizontally placed circular steel tube. Their experimental outcome depicted a significant enhancement in the HTC of the nanofluids during the single-phase region of boiling, with an increase in the nanoparticle concentration. However, a considerable decrease in the HTC was recorded with the increase in the volume concentration during the subcooled flow boiling regime. Paul et al. [60] investigated the flow boiling of water-based Al_2O_3 nanofluids in vertical bottom flooded tubes and focused on deriving the Leidenfrost temperature and heat flux from the temperature readings recorded. Their results demonstrated the enhancement in the CHF with the addition of the nanoparticles in the water. Their results presented nanoparticle deposition activity caused by early quenching, leading to the enhanced CHF. The impact of the initial temperature of the tube was studied on the heat flux with a mass flow rate of 0.02667 kg/s at 580 mm from the bottom of the tube. Figure 13 presents the boiling curves of the water and nanofluids, and an increase in the CHF can be seen with the increase in the initial temperature.

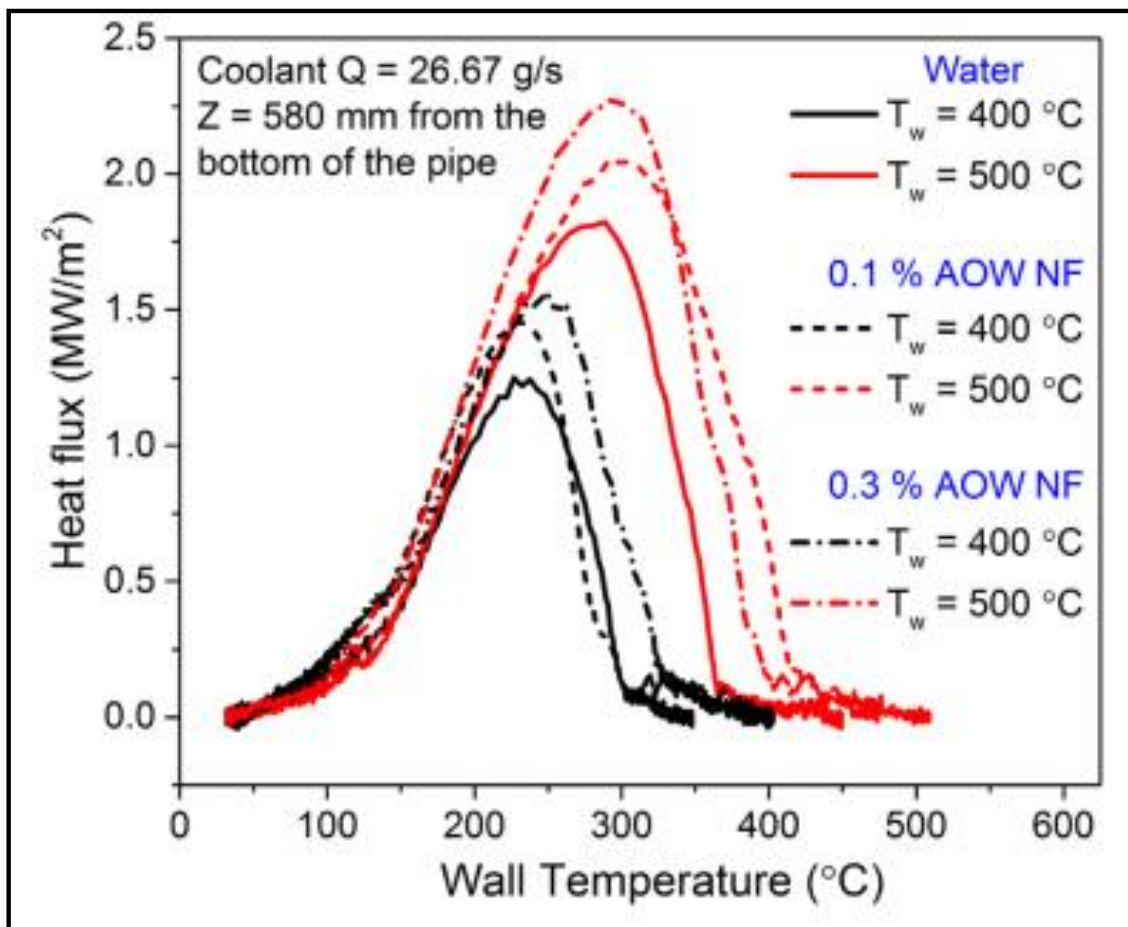


Figure 13. Effect of the initial temperature on the boiling performance of water and Al₂O₃–water nanofluids. Reproduced with permission from [60]. Elsevier, 2016.

Zangeneh et al. [61] performed the forced convective and subcooled flow boiling of functionalized ZnO–water nanofluids in a vertical annulus. Their results demonstrated high heat transfer performance in the ZnO nanofluids when compared to water for both tested regions. Sarafraz et al. [62] performed flow boiling experiments of water and CuO–water nanofluids in an annular space at varying operating conditions. Their results demonstrated significant enhancement in the HTC, with increasing applied heat flux and flow rate during both forced convective and nucleate boiling regimes. Their results confirmed that the fluid inlet temperature was one of the important parameters in the HTC enhancement, especially during the nucleate boiling regime.

Setoodeh et al. [63] performed an innovative study on subcooled flow boiling of water-based Al₂O₃ nanofluids at a particular volume fraction. Their test rig consisted of a circular hot spot aluminum surface fixed at the end of a rectangular channel, as shown in Figure 14. The hot spot was used to heat the inflow of the nanofluids. The results demonstrated an increase in the boiling performance with the increase in the surface roughness and stream velocity. They concluded that the nanofluids exhibited an increased forced convective and flow boiling HTC when compared to water.

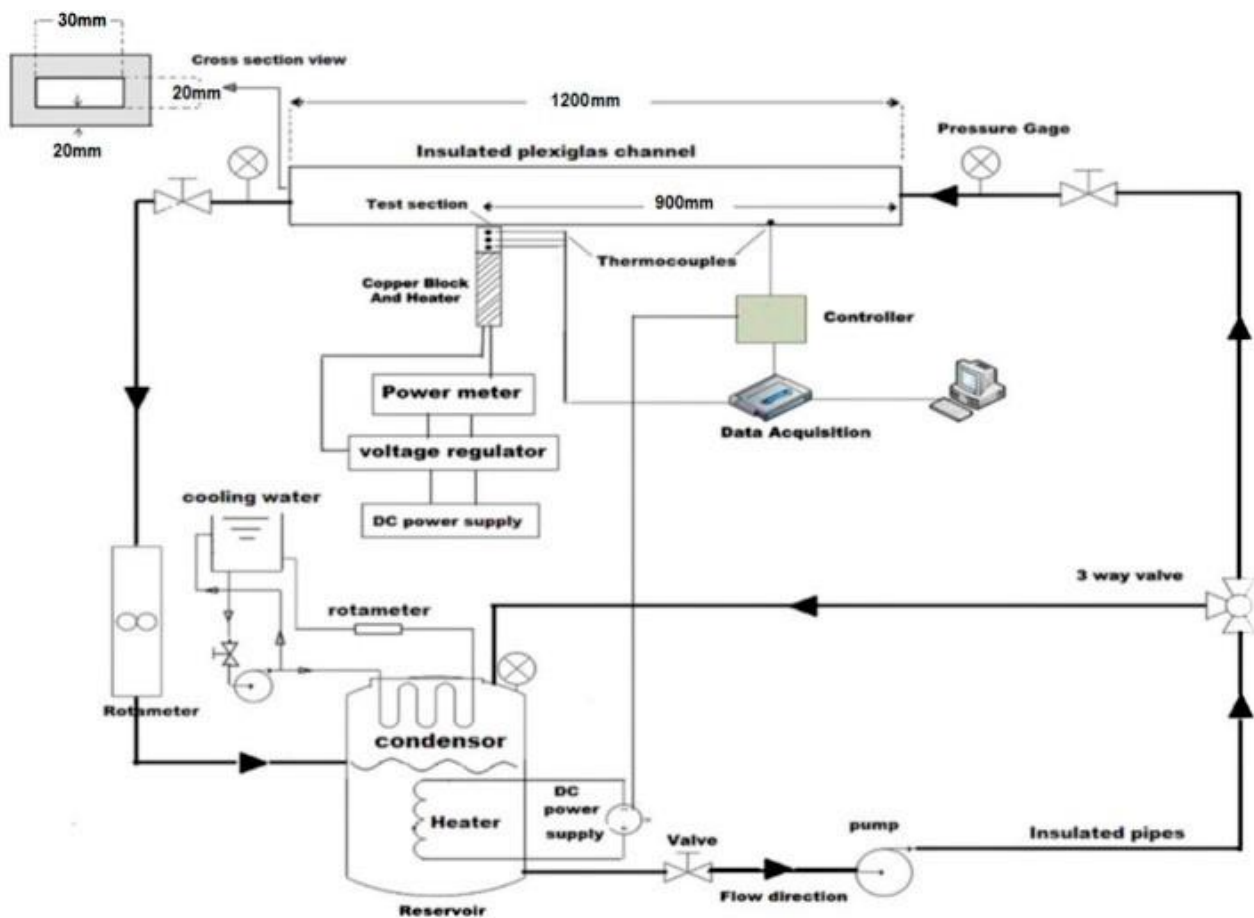


Figure 14. Flow boiling experimental setup used by Setoodeh et al. [63]. Reproduced with permission from [63]. Elsevier, 2015.

Sarafraz and Hormozi [64] studied the flow boiling heat transfer characteristics of water-based CuO, Al₂O₃, and MWCNT dispersions in a vertical annulus. They investigated the impacts of varying operating conditions on the heat transfer performance and thermal fouling resistance parameters by altering the nanoparticle concentration, heat flux, and mass flux. Their results demonstrated an increase in the HTC of nanofluids with the increase in the nanoparticle concentration, heat flux, and mass flux. Figure 15 verifies that the MWCNT nanofluids depicted the best boiling performance and a lower fouling resistance value, when compared to the other nanofluids used in this study.

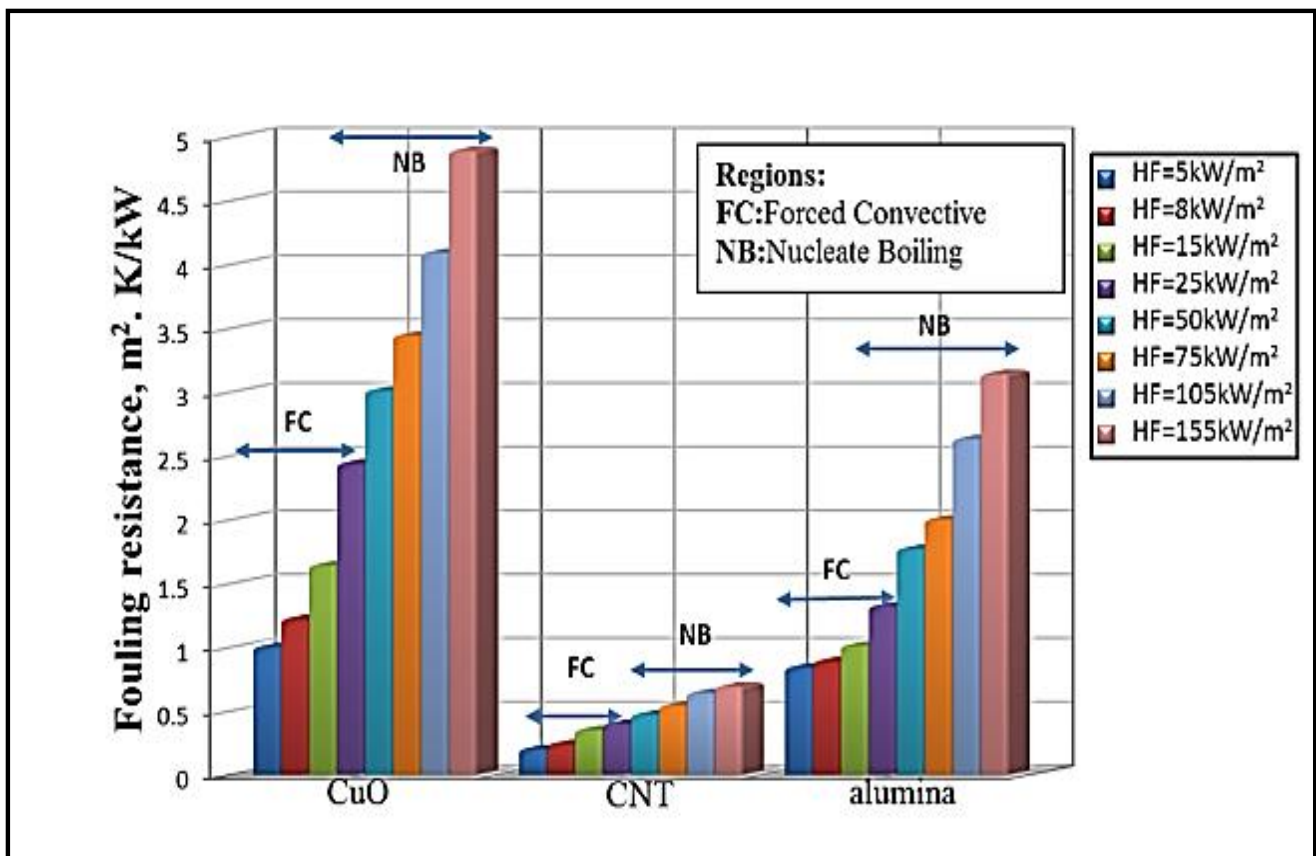


Figure 15. Fouling resistance and boiling performance of CuO, CNT, and Al₂O₃ nanofluids. Reproduced with permission from [64]. Elsevier, 2016.

Rana et al. [65] investigated the subcooled flow boiling of water-based ZnO nanofluids at low concentrations (≤ 0.01 vol%) in a horizontal annulus test section made of a borosilicate glass tube. The nanofluid flow was heated with a 780 mm-long electrically heated rod inserted into the test section. The bubble behavior in the nanofluid flow boiling was studied by the optical method. The parametric effect of the particle volume fraction of ZnO, flow rate, and heat flux on the bubble behavior was reported. The experiment was carried out by changing the heat flux ranging from 100 kW/m² to 450 kW/m² and flow rates from 0.1 L/s to 0.175 L/s at a 1bar inlet pressure and at a constant subcooling temperature of 20 °C. Visualization results were obtained by capturing bubble images using a high-speed video camera and analyzed with the National Instruments IMAQ Vision Builder 6.1 image processing software. Their results indicated that the increase in heat flux led to an increase in bubble diameter. The bubble diameter and bubble density decreased in the water and nanofluids, with an increase in the flow rate. An enhancement in the HTC was observed with the increase in the volume fraction of the ZnO nanoparticles and heat flux.

Lee et al. [66] investigated the heat transfer performance in the flow boiling of water-based Al₂O₃ and SiC nanofluids at 0.01 vol.% flowing upward inside a vertical 12.7 mm stainless steel tube under low-pressure and low-flow (LPLF) conditions. Four mass fluxes of 100 kg/m²s, 150 kg/m²s, 200 kg/m²s, and 250 kg/m²s and two inlet temperatures of 25 °C and 50 °C were selected in the experiment. They stated that the CHF enhancements varied with mass flux and fluid inlet temperature. Their results demonstrated a 15% and 41% enhancement in the CHF for the Al₂O₃ and SiC nanofluids, respectively. The improvement in the CHF for the SiC nanofluid was mainly due to its significantly high thermal conductivity when compared to Al₂O₃. The surface contact angle measurements for the SiC nanofluid was less than that of the Al₂O₃ nanofluid. The SEM observations showed that the nanoparticle deposits on the heated surface were the prime reason for the

observed lower contact angles, which effectively modified the surface wettability, leading to a delay in the liquid film dryout, causing the enhancement of the CHF.

Vafaei et al. [67] carried out the transient boiling heat transfer analysis of water and alumina–water nanofluid. They suggested that the nanoparticles played an important role in enhancing the CHF during flow boiling heat transfer through surface modifications caused by nanoparticle deposition and changes in the bubble dynamics caused by suspended nanoparticles in the fluid. Afterwards, Vafaei and Wen [68] reported further studies and the appraisal of the legitimacy of various microchannel-based CHF correlations developed using experimental data. With the estimation of all the CHF correlations, the Lee and Mudawar model [69] depicted the best results with a mean absolute error of 34%.

A summary of the research work on flow boiling is presented in Table 5.

Table 5. Summary of experimental research on flow boiling in nanofluids.

References	Nanofluids; Particle Size (nm and μm) and Concentration	The Geometry and Material of the Test Section; Dimension/Diameter (mm); Length (mm)	Flow Parameters: Pressure System (kPa)/d (mm)/ q (kW/m^2)/ G ($\text{kg}/\text{m}^2\text{s}$)	Results of (HTC/CHF) of Flow Boiling Using Nanofluids
Afrand et al. [7]	TiO ₂ –DI water; 20 and 40; 1–3 vol% Al ₂ O ₃ ; 20 and 40; 1–3 vol%	Vertical and horizontal stainless steel circular tube; 10; 1000	150/37.5–705/137–412	Degraded for both the vertical and horizontal tube with the presence of nanoparticles
Sarafraz et al. [55]	MgO–Therminol; 66; 50; 0.1 and 0.3 mass%	Stainless steel chamber with a copper disk with horizontal surface; 10 (diameter of copper disk)	101/30–700	Improvement of about 23.7% for 0.1 mass%.
Karimzadehkhoei et al. [56]	γ Al ₂ O ₃ –distilled water; 20; 0.01–1.5 mass%	Horizontal stainless steel microtube; 0.502; 70 and 120	101/220–600/1200–3400	Deteriorated with high concentration
Hashemi et al. [57]	MWCNT–water; D = 10–20 nm and L = 30 μm ; 0.001 and 0.01 mass%	Horizontal stainless steel circular tube; 10; 2000	101/60–200/320–920	Improved for both water and nanofluids with increasing heat flux and mass flux/enhanced for flow boiling of nanofluid
Choi et al. [58]	Fe ₃ O ₄ –DI water; 25; 0.01 vol%	Vertical stainless circular steel tube; 10.92; 250	100/1000–5000	Enhanced up to 40% for nanofluid compared to water
Rajabnia et al. [59]	TiO ₂ –distilled water; 20; 0.01–0.5 vol%	Horizontal stainless steel circular tube; 10; 1000	101; 26–102; 138–308	Deteriorated with nanoparticles for the two-phase regime (subcooled boiling flow)
Paul et al. [60]	Al ₂ O ₃ –water; 26; 0.1; 0.3 vol%	Vertical stainless steel circular tube; 11.5; 1500	100; 0–2000; 125–453	Enhanced with nanofluid compared to water, and this enhancement increased with the concentration of particles
Zangeneh et al. [61]	ZnO–DI water; less than 50; 0.005–0.02 vol%	Vertical annulus channel; 20; 150	100; 8–110; 23–50	Improved with ZnO–water nanofluids
Sarafraz et al. [62]	CuO–DI water; 50; 0.1–0.3 mass%	Vertical stainless steel annular tube; 30; 300	101; 50–132; 0–400	Improved with increasing mass flow rate of fluid
Setoodeh et al. [63]	Al ₂ O ₃ –DI water; 20–30; 0.001–0.1 vol%	Aluminum circular surface in the bottom of Plexiglas channel; 12; 300	120; 0–5500; 490–880	Augmented with surface roughness and mass flow rate
Sarafraz and Hormozi [64]	CuO–DI water; 50; 0.1–0.3 mass% Al ₂ O ₃ ; 50; 0.1–0.3 mass% MWCNT 0.1–0.3 mass%	Vertical annulus channel; 30; 300	100; 0–175; 400–1200	Enhanced for MWCNT compared to other nanofluids with increasing mass and heat fluxes
Rana et al. [65]	ZnO–water; 40; 0.001–0.01 vol%	Horizontal annulus made of borosilicate glass tube and stainless steel rod; 21.8; 500	101/21.8/500/405–710/100–550	Enhanced with increasing concentration
Lee et al. [66]	Al ₂ O ₃ , SiC–water; more or less than 50; 0.01 vol%	Vertical stainless round tube; 12.7(t); 500	101/12.7/500/100–250/100–3500	Enhancement of 15% for Al ₂ O ₃ –water
Vafaei and Wen [67]	Al ₂ O ₃ –water; 25; 0.001–0.1 vol%	Stainless steel microchannels; 0.51; 0.16(t); 306	101/0.51/306/600–1950/175	Modest enhancement under very low concentrations
Balasubramanian et al. [70]	Al ₂ O ₃ –DI water; 40–50; 0.01–0.1 vol%	31 parallel U-shaped copper microchannels; 0.308; 30	101/1100–4450/100–800	Enhanced during the transient state/enhanced up to 15% for moderate volume concentration

Table 5. Cont.

References	Nanofluids; Particle Size (nm and μm) and Concentration	The Geometry and Material of the Test Section; Dimension/Diameter (mm); Length (mm)	Flow Parameters: Pressure System (kPa)/d (mm)/q (kW/m ²)/G (kg/m ² s)	Results of (HTC/CHF) of Flow Boiling Using Nanofluids
Abedini et al. [71]	TiO ₂ -DI water; 10 and 20; 0.1–2.5 vol% Al ₂ O ₃ -water; 10 and 20; 0.1–2.5 vol% CuO-water; 10 and 20; 0.1–2.5 vol%	Vertical stainless steel circular tube; 10; 1000	101/13–76.5/37–210	Improved in single-phase regime and deteriorated with two-phase regime using nanofluids
Patra et al. [72]	Al ₂ O ₃ -DI water; 20–25; 0.001–0.01 vol% TiO ₂ ; 30–38; 0.001–0.01 vol%	Vertical annulus channel; 33; 880	101/30–250/4–10	Increased with dilute concentration
Zhang et al. [73]	GO-water; 500–1000; 0–0.05 mass%	Horizontal copper microchannels; 2.5 width and 0.5 height	101/0–100/0.04–0.07	Decreased/enhanced
Zhang et al. [74]	MWCNT-R123; D = 30–70 nm and L = 2–19 μm ; 0.02–0.2 vol%	Horizontal copper circular tube; 9; 2000	100; (2*); 300–500	Enhanced with increase concentration, mass flux, and vapor quality
Tazarv et al. [75]	TiO ₂ -R141b; 20; 0.01–0.3 vol%	8.825; 2250	101; 1–28; 192–482	Improved for nanorefrigerant compared to pure refrigerant
Wang et al. [76]	γ Al ₂ O ₃ -DI water; D = 20 nm and L = 50 nm; 0.1–0.5 vol%	Vertical stainless steel circular tube; 6; 1100	200–800; 50–300; 350–1100	Enhanced using nanofluid
Salari et al. [77]	Al ₂ O ₃ -DI water; (5, 50 and 80); 0.5–0.1 vol%	Vertical annulus channel; 30; 150	100; 0–85; 400–600	Enhanced for short-time study and deteriorated for long-time study
Soleimani et al. [78]	Al ₂ O ₃ -DI water; 20–30; 0.1; 0.25 vol%	Plexiglas channel with rectangle shape; 20×30; 1200	120; 0–700; 400–850	Enhanced using nanofluid
Moreira et al. [79]	Al ₂ O ₃ -DI water; 20–30; 0.001–0.1 vol%	Horizontal stainless steel tube; 1.1; 200	101; 100–400; 200–600	Improved with low concentration and decreased with high concentration
Lee et al. [80]	Fe ₃ O ₄ -water; Al ₂ O ₃ -water; 20–30; 0.01–0.1 vol%	Vertical stainless tube; 10.92; 250	110/10.92/250/100–500/a	Enhanced drastically using Fe ₃ O ₄ -water
Xu and Xu [81]	Al ₂ O ₃ -water; 40; 0.2 wt%	Microchannel test section made of Pyrex glass and silicon wafer; 0.143; 7.5	101/0.143/7.5/171–401/0–1000	17% enhancement

6.2. Analytical and Numerical Work

Flow boiling in nanofluids is turning into a fascinating topic of research. However, analytical and numerical mathematical investigations concerning the flow boiling heat transfer are limited. In this review, some important correlations were briefly discussed. Table 6 summarizes recent analytical and numerical work on the flow boiling heat transfer in nanofluids. Wang et al. [82] investigated the flow boiling CHF of water-based Al₂O₃ and AlN nanofluid with 0.1–0.5 vol.% inside a vertical channel. They examined the parametric impacts on the CHF by varying the mass and heat fluxes, system pressure, subcooling temperature, nanoparticle type, and concentration. They also discussed the mechanism involved in the nanoparticle deposition activity on the heated surface and the effect on the boiling and CHF of nanofluids. Their results demonstrated an increase in the CHF with the increase in mass flux, diameter of the channel, and pressure system. The CHF enhanced up to 18% when compared to conventional fluid. At the same time, the impacts of different types of nanoparticles and the change in the concentration and subcooling temperature did not impart any noticeable change in the CHF. Finally, they developed a CHF correlation as mentioned below.

$$q_{CHF} = \Delta T_{sub} C_p G \left(\frac{D_{in}}{4L} \right) + 0.7073 G h_{fg} \left(\frac{D_{in}}{L} \right)^{0.9708} \left(\frac{\rho_g}{\rho_l} \right)^{0.2013} \left(\frac{(\rho_l - \rho_g)^{0.5} u^2}{g^{0.5} \sigma^{0.5}} \right)^{-0.1135} \quad (6)$$

The proposed correlation accurately predicts a range of parameters D_{in} (6–8 mm), heating length l (500–800 mm), inlet subcooled temperature ΔT_{sub} (13.5–35.9 °C), pressure system $P = 400$ –890 (kPa), and mass flux $G = 98.9$ –348.4 ($\text{kg m}^{-2} \text{s}^{-1}$).

Rabiee et al. [83] simulated the dryout phenomenon of a nanofluid inside a reactor rod bundled with mixing vanes. The Reynolds-averaged Navier–Stokes (RANS) equations were solved in a Eulerian–Eulerian two-phase framework to efficiently model the boiling flow field, and some constitutional relations were used to present the CHF during the boiling phenomenon in equilibrium and non-equilibrium conditions. By simulating with alumina nanoparticles, they noticed that the nanoparticles in the base fluid delayed the quick changes in the wall temperature even with the presence of mixing vanes attached to the spacer grid. The maximum temperature at the wall was reduced in the presence of the mixing vanes. They noticed that the HTC was nearly the same until the liquid contacted the heated wall before the CHF region, besides a sharp drop in the boiling crisis area. The authors reported that in certain nanoparticle concentrations (in their case, an 8–9 vol.% of alumina nanoparticles), film boiling would (and exerted) improve wall heat flux with a 9.4% enhancement of the base heat flux for the occurrence of the dryout phenomenon. Therefore, nanoparticles inclusion in the base fluid can positively result in heat removal enhancement and improve the CHF threshold. At the same time, disadvantages such as sedimentation, etc., would occur. Most importantly, the nanofluid could postpone the dryout phenomenon, and that could potentially be a major advantage in applications, in particular under accident conditions.

Abedini et al. [84] used the mixture model to simulate the subcooled flow boiling of water-based Al_2O_3 (30 nm) nanofluids in a vertical concentric annulus and vertical tube. The K - ϵ model was utilized to develop the turbulence of the fluid. Flow boiling characteristics such as the axial volume fraction and temperature distribution were anticipated, and the results were in very good agreement with the literature. Accordingly, the model was able to accurately predict the temperature distribution and axial vapor volume fraction. The authors investigated the change in the vapor volume fraction at the inlet for a constant velocity and mass flux, to present a comparison for different concentrations. The authors concluded that quenching and evaporation were two important factors in subcooled flow boiling, due to which higher a heat transfer at a lower inlet velocity was possible in some states. At a constant inlet velocity, the increase in the nanoparticle concentration caused a decrease in the axial volume fraction of the vapor, which brought about a decrease of the wall temperature.

Esfe et al. [85] developed a numerical model to predict the heat transfer and pressure drop of Ag–water nanofluid with volume fractions up to 1% as in a double-tube heat exchanger applying a multi-objective artificial neural network (ANN). New correlations for determining the relative Nusselt number and relative pressure drop were established. The nanofluid concentration and Reynolds number were considered as the inputs to the network. The network outlines revealed that the relative pressure drop and Nusselt number were independent of the Reynolds number, and they were a function of the nanoparticle volume only. Despite the noisy data, the designed neural network calculated the regression coefficients for the relative pressure drop and relative Nusselt number as 99.54% and 99.76%, respectively, which showed that the neural network was highly accurate and could be used as an efficient tool to reduce the expenses in experiments with various thermal systems.

Wang et al. [86] developed a mathematical model for the flow boiling of water-based AlN and Al_2O_3 nanofluids. They utilized several dimensionless parameters to demonstrate the model as a function of heat flux, mass flux, and the pressure system on flow boiling using nanofluids. They proposed the model with a mean absolute deviation of 4.3% and had a 99% prediction capability with a $\pm 15\%$ accuracy for AlN nanofluids and the same, with a 94.5% prediction capability with a $\pm 15\%$ accuracy, for Al_2O_3 nanofluids. The parameters estimated in the proposed model had concentrations ranging from 0.1–0.5 vol%,

a system pressure from 200–800 kPa, a heat flux from 48–289 kW/m², and a mass flux from 350–1100 kg/m²s.

$$Nu = 1.1817 \left(\frac{q'' D_{in}}{\mu_{nf} h_{fg}} \right)^{0.1814} \left(\frac{\mu_{nf} C_{p,nf}}{k_{nf}} \right)^{4.1506} \left(\frac{\rho_1}{\rho_v} \right)^{0.8871} \quad (7)$$

where,

$$Nu = \frac{h_{nf} D_{in}}{k_{nf}} \quad (8)$$

Rakhsha et al. [87] performed both numerical and experimental investigations on the turbulent forced convection flow of water-based CuO nanofluids with concentrations of 0.1 vol.% and 0.2 vol.%, in helical coiled tubes at a constant wall temperature to examine the pressure drop and convective heat transfer behavior, and the data were compared to those for pure water. The numerical analysis was performed by solving the governing equations by virtue of the finite-volume method in Open FOAM. The results demonstrated a 6–7% enhancement in the HTC and a 9–10% increase in the pressure drop with CuO nanofluid over pure water. However, the experimental results showed a 16–17% increase in the HTC; an enhancement of 14–16% was noticed in the pressure drop for different geometrical tubes and different Reynolds numbers. Therefore, the analytical results depicted very small increments when compared to the experimental results. The results demonstrated that the pressure drop and HTC increased as the curvature ratio and Re number increased. Finally, the authors proposed a relevant model using the numerical and the experimental data to predict the friction factor coefficient and Nusselt number.

Aminfar et al. [88] introduced a numerical work examining the impacts of a non-uniform axial magnetic field with positive and negative gradients on subcooled nanofluid flow boiling using the refrigerant R-113-based Ferro fluid consisting of 4 vol.% Fe₃O₄ particles of 10 nm in diameter. At first, the single-phase convection was analyzed. The control volume approach for separate governing equations, the SIMPLEC algorithm for pressure-velocity coupling, and the SST k- ω model for turbulent flow were used separately. Then, a three-dimensional two-fluid model was applied to determine subcooled flow boiling, and the R-113 boiling experimental data obtained were used to verify the results. Their results demonstrated that nanofluid usage and the application of a non-uniform axial magnetic field had significant impacts on single-phase convection, as well as subcooled flow boiling. Magnetic fields with negative gradients depicted an increase in the single-phase convection heat transfer rate and an increase in the CHF due to the reduced evaporation rate on the wall surface, which eventually led to a wall dryout. Thus, a safer operational condition of industrial equipment can be developed.

Sasmito et al. [89] conducted a numerical analysis of heat transfer enhancement in nanofluid flow inside a coiled square tube under a laminar region. Water-based Al₂O₃ and CuO nanofluids with concentrations of 0%, 1%, 2%, and 3% were taken as the working fluids, and the flow behavior and heat transfer performance of those fluids were evaluated in coiled square tubes with different configurations such as straight, conical spiral, in-plane spiral, and helical spiral. Their results showed the computational fluid dynamics (CFD) simulation for the laminar flow inside the coils of a square cross-section. The properties of the nanofluid were considered as a function of the volumetric concentrations and temperature. Their results demonstrated significant enhancement in heat transfer performance with the addition of small amounts of nanoparticles up to 1%, and the further addition of nanoparticles displayed a deterioration of the heat transfer performance. Al₂O₃ nanofluids displayed 5% better heat transfer performance when compared to CuO nanofluids.

Table 6. Summary of analytical or numerical studies on flow boiling in nanofluids.

References	Nanofluids; Particle Size (nm and μm) and Concentration	Topic/Method of Simulation	The Geometry and Material of the Test Section Dimension/Diameter (mm/nm/ μm); Length (mm/nm/ μm) Flow Parameters: Pressure System (kPa)/d (mm)/G (kg/ m^2s)	Results of Flow Boiling Nanofluids
Abedini et al. [71]	Al_2O_3 -water; 30 nm; 1, 2 and 4 vol%	Prediction of the axial vapor volume fraction of a nanofluid in the subcooled flow boiling /two-phase mixture model	A circular tube and an annulus; 1.37 bar, 1.65 bar, and 1 bar; 156.15 kg/ m^2s , 634.5 kg/ m^2s , 1115.0 kg/ m^2s , 1500–2500 kg/ m^2s	The model could predict the axial vapor volume fraction and temperature distribution well; at a constant inlet velocity of nanofluids, the increase in concentration caused a decrease in the axial volume fraction of vapor; at a constant inlet mass flux, the axial vapor volume fraction was higher compared to the previous case due to the lower velocity of the nanofluid
Rabiee et al. [83]	Al_2O_3 -water; 8–9 vol%	Influence of alumina nanoparticles on critical heat flux (CHF) and dryout phenomenon/Eulerian–Eulerian framework, RPI model, FLUENT	A single vertical channel of a typical PWR with 17×17 fuel assemblies in which rod bundles are arrayed in an 8×8 pattern	Improved heat removal enhancement; improve CHF; postponed dryout phenomenon; caused sedimentation and fouling
Abedini et al. [84]	Al_2O_3 -water; 30 nm; 1, 2 and 4%	Numerical investigation of subcooled flow boiling/two-phase mixture model, k- ϵ model	Tube and annulus; 1–2.69 atm; 156.15–2500 kg/ m^2s ;	Increasing concentration of nanoparticles enhanced the heat transfer; A lower concentration of nanoparticles (1–2%) was more effective than a higher concentration (4%) on the HTC; increasing the inlet mass flow rate, may increase or decrease the HTC; Specific heat and viscosity did not have a significant effect on the HTC
Esefe et al. [85]	Ag-water; 30 nm and 50 nm; 0.125, 0.25, 0.5, 0.75, and 1 vol%	Neural network design for predicting the heat transfer and pressure drop characteristics/ multi-objective artificial neural network modeling	A double-tube heat exchanger with a pipe length of 111 cm	The relative pressure drop and Nusselt number were independent of the Reynolds number, but they depended on the nanoparticle volume fraction; the developed model was able to predict the pressure loss and Nusselt number for heat exchangers using nanofluids with high accuracy

Table 6. Cont.

References	Nanofluids; Particle Size (nm and μm) and Concentration	Topic/Method of Simulation	The Geometry and Material of the Test Section Dimension/Diameter (mm/nm/ μm); Length (mm/nm/ μm) Flow Parameters: Pressure System (kPa)/d (mm)/G (kg/ m^2s)	Results of Flow Boiling Nanofluids
Wang et al. [86]	Al_2O_3 -water; 20–56 nm; 1.0, 2.0, 3.0 and 4.0 vol%	Numerical simulation on bubble dynamics' behavior during flow boiling/ moving particle semi-implicit method (MPS-MAFL)	0.1 MPa	Bubbles grew faster, and along with bubble departure, the frequency increased with increasing volume concentration of nanofluids; The nanofluid with a nanoparticle diameter of 29 nm showed a maximum value; an optimal nanoparticle diameter range was suggested between 20 nm and 38 nm for water/ Al_2O_3 nanofluids
Rakhsha et al. [87]	CuO -water; 68 nm; 0.1 and 0.2 vol%	Investigations on turbulent forced convection flow/Open FOAM Version 2.1.2.	A horizontal coiled tube with a heating tank of 40 cm * \times 60 cm \times 40 cm cubic chamber made of 2 mm stainless steel plate.	Experimental results predicted an enhancement of the pressure drop and heat transfer for water 14–16% and 16–17%, respectively; numerical simulation predicted only 6–7% and 9–10% enhancements for water in the pressure drop and heat transfer, respectively; correlations developed
Aminfar et al. [88]	Fe_3O_4 -R113; 10 nm; 4 vol%	Numerical study of non-uniform magnetic fields' effects/control volume technique, SIMPLEC algorithm, SST k- ω model, a three-dimensional two-fluid model	A stainless-steel, Plexiglass-, and optical-quartz-made, straight vertical annulus with ID 15.87 mm, OD 38.02 mm, length 3.66 m; 2.69 bar; 784 kg/ m^2s	Single-phase convection heat transfer rate increased; CHF in the subcooled boiling flow increased
Sasmito et al. [89]	Al_2O_3 -water, CuO -water; 0, 1, 2 and 3%	Numerical evaluation of laminar passive heat transfer enhancement/computational fluid dynamics (CFD)	Coiled square tubes with 4 different configurations (straight, conical spiral, in-plane spiral, and helical spiral)	The addition of small amounts of nanoparticles improved the heat transfer performance up to 1%; further addition deteriorated the performance; Al_2O_3 nanofluids gave higher heat transfer (approximately 5%) than CuO nanofluids
Purbia et al. [90]	Graphene-water; 0.025%, 0.05%, 0.075%, 0.1%	Modeling and simulation for two-dimensional steady-state momentum transfer and heat energy consumption/MATLAB R2018b	A rectangular enclosure with 100 \times 100 grids; three different inlet velocities (0.5 m/s, 1 m/s, and 1.5 m/s)	Thermal performance at turbulent condition was higher than the base fluid (2–300%) at higher concentrations; dramatic reduction in the operating cost

Table 6. Cont.

References	Nanofluids; Particle Size (nm and μm) and Concentration	Topic/Method of Simulation	The Geometry and Material of the Test Section Dimension/Diameter (mm/nm/ μm); Length (mm/nm/ μm) Flow Parameters: Pressure System (kPa)/d (mm)/G (kg/ m^2s)	Results of Flow Boiling Nanofluids
Tafarroj et al. [91]	TiO ₂ -water; 0.5, 1, and 2 vol%	Prediction of the HTC and Nusselt number during flow /artificial neural network modeling (ANN) for predicting the HTC (23 datasets) and Nusselt number (72 datasets)	40 microchannels, each having a length of 4 cm, width 500 μm , height 800 μm ; two values of the Reynolds number, i.e., 400 and 1200	The ANN was able to produce convincing results of the HTC with 0.2% relative error and Nusselt number values with 0.3% relative error
Mohammad pourfard et al. [92]	Fe ₃ O ₄ -water; 0.1 vol%	Study of the influence of magnetic-field-induced centrifugal force on flow boiling	A vertical annulus with 0 mm, 1 mm, 2 mm, and 4 mm heights of twisted fins, ID 4 mm, OD 12 mm, thickness 0.05 mm, length of channel 500 mm; 5 MPa; 311 kg/ m^2s	Inserting a spiral fin into the inner wall of the annulus enhanced the rate of convective heat transfer and decreased the evaporative mass flux; the application of a transverse non-uniform magnetic field provided additional enhancement in the CHF

7. Conclusions and Future Direction

A systematic review of the results relating to nanofluid applications in plasma-facing components and Hyper Vaportrons were described here. The nanofluid mainly undergoes boiling or two-phase heat transfer during the selected application. Thus, the results of pool and flow boiling heat transfer in nanofluids were also discussed in this paper. Based on the discussions, the following conclusions can be reached:

- The cooling performance of PFCs and HVs can be increased with the application of nanofluids. A very small amount of particle addition yields better heat transfer form PFCs and HVs. However, the mechanism of heat transfer enhancement is not properly known and still needs more investigation;
- The cooling of PFCs and HVs is mainly driven by boiling or two-phase heat transfer. The boiling in nanofluids depends on several factors and their combined effects. The addition of nanoparticles causes HTC and CHF enhancements in nanofluids, but excessive particle addition is detrimental and results in a decline in heat transfer, even lower than base fluid. Therefore, there is an optimum nanoparticle concentration that should be added for considerable heat transfer enhancement;
- The boiling heat transfer in nanofluid is controlled by the change in the topography and surface structure of the heating surface due to nanoparticle deposition activity. The change in the heating surface microstructure brings about changes in the surface characteristics such as wetting, roughness, and capillary wicking, which are very much responsible for heat transfer in nanofluids. The dominant nature of thermal conductivity enhancement and the development of active nucleation sites also play responsible roles in the heat transfer enhancement in nanofluids;
- The application of nanofluids particularly in fusion cooling is very limited. This may be due to the lesser understanding of the underlying complex phenomena in Hyper Vapotron technology. Therefore, more studies in this regard are critical. Besides this, Al₂O₃ nanofluids are frequently selected for cooling applications. However, other materials should be applied to reach any conclusion;

- Bubble formation and bubble dynamics are key mechanisms of the boiling heat transfer in nanofluids. More experiments should be conducted to understand these mechanisms properly;
- The effect of the pressure system on flow boiling in nanofluids has not been studied properly. Therefore, research on this topic needs serious attention. Boiling heat transfer on nanocoated surfaces also needs further attention in future research.

Finally, nanofluids seem to be promising for the cooling of plasma-facing components and Hyper Vaportrons. However, there are some critical issues with nanofluids such as stability, scale formation, production cost, and compatibility.

Author Contributions: Conceptualization, data collection and representation, writing original draft—S.M. Writing original draft, editing and data collection—S.E. Supervision, editing, analysis, initial review—N.A., P.C.M. Supervision, data collection, review and conceptualization—P.C. All authors have read and agreed to the published version of the manuscript.

Funding: No external finding was received for this work.

Institutional Review Board Statement: Not applicable for this work.

Informed Consent Statement: Not applicable for this work.

Data Availability Statement: Not applicable for this work.

Conflicts of Interest: The authors do not have any conflict of interest.

References

1. Choi, S.U.S.; Eastman, J.A. *Enhancing Thermal Conductivity of Fluids with Nanoparticles*; Argonne National Lab.: Lemont, IL, USA, 1995.
2. Maddah, H.; Rezazadeh, M.; Maghsoudi, M.; NasiriKokhdan, S. The effect of silver and aluminum oxide nanoparticles on thermophysical properties of nanofluids. *J. Nanostruct. Chem.* **2013**, *3*, 28. [CrossRef]
3. Abdelrazek, A.H.; Alawi, O.A.; Kazi, S.N.; Yusoff, N.; Chowdhury, Z.; Sarhan, A.A.D. A new approach to evaluate the impact of thermophysical properties of nanofluids on heat transfer and pressure drop. *Int. Commun. Heat Mass Transf.* **2018**, *95*, 161–170. [CrossRef]
4. Estellé, P.; Halelfadl, S.; Maré, T. Thermophysical properties and heat transfer performance of carbon nanotubes water-based nanofluids. *J. Therm. Anal. Calorim.* **2017**, *127*, 2075–2081. [CrossRef]
5. Kole, M.; Dey, T.K. Investigations on the pool boiling heat transfer and critical heat flux of ZnO-ethylene glycol nanofluids. *Appl. Therm. Eng.* **2012**, *37*, 112–119. [CrossRef]
6. Sarafraz, M.M.; Hormozi, F. Pool boiling heat transfer to dilute copper oxide aqueous nanofluids. *Int. J. Therm. Sci.* **2015**, *90*, 224–237. [CrossRef]
7. Afrand, M.; Abedini, E.; Teimouri, H. Experimental investigation and simulation of flow boiling of nanofluids in different flow directions. *Phys. E Low Dimens. Syst. Nanostruct.* **2017**, *87*, 248–253. [CrossRef]
8. Cheng, L.; Liu, L. Boiling and two-phase flow phenomena of refrigerant-based nanofluids: Fundamentals, applications and challenges. *Int. J. Refrig.* **2013**, *36*, 421–446. [CrossRef]
9. Mir, S.; Akbari, O.A.; Toghraie, D.; Sheikhzadeh, G.; Marzban, A.; Mir, S.; Talebizadehsardari, P. A comprehensive study of two-phase flow and heat transfer of water / Ag nanofluid in an elliptical curved minichannel. *Chin. J. Chem. Eng.* **2020**, *28*, 383–402. [CrossRef]
10. Solangi, K.H.; Kazi, S.N.; Luhur, M.R.; Badarudin, A.; Amiri, A.; Sadri, R.; Zubir, M.N.M.; Gharekhani, S.; Teng, K.H. A comprehensive review of thermo-physical properties and convective heat transfer to nanofluids. *Energy* **2015**, *89*, 1065–1086. [CrossRef]
11. Sergis, A.; Hardalupas, Y.; Barrett, T.R. Isothermal analysis of nanofluid flow inside HyperVaportrons using particle image velocimetry. *Exp. Therm. Fluid Sci.* **2018**, *93*, 32–44. [CrossRef]
12. Mukherjee, S.; Mishra, P.C.; Chaudhuri, P.; Bhattacharjee, H. Energy Viability Analysis of AL₂ O₃ /Water Nanofluid Flow Applied as Coolant in Nuclear Applications. Available online: <https://nucleus.iaea.org/sites/fusionportal/Shared%20Documents/FEC%202018/fec2018-preprints/preprint0325.pdf> (accessed on 3 December 2021).
13. Sergis, A.; Hardalupas, Y.; Barrett, T.R. Potential for improvement in high heat flux HyperVapotron element performance using nanofluids. *Nucl. Fusion* **2013**, *53*, 113019. [CrossRef]
14. Sezer, N.; Atieh, M.A.; Koç, M. A comprehensive review on synthesis, stability, thermophysical properties, and characterization of nanofluids. *Powder Technol.* **2019**, *344*, 404–431. [CrossRef]
15. Oumer, A.N.; Chen, J.L.T.; Azizuddin, A.A. A review on thermo-physical properties of bio, non-bio and hybrid nanofluids. *J. Mech. Eng. Sci.* **2019**, *13*, 5875–5904.

16. Rudyak, V.Y.; Minakov, A.V. Thermophysical properties of nanofluids. *Eur. Phys. J. E* **2018**, *41*, 15. [[CrossRef](#)]
17. Gupta, M.; Singh, V.; Kumar, R.; Said, Z. A review on thermophysical properties of nanofluids and heat transfer applications. *Renew. Sustain. Energy Rev.* **2017**, *74*, 638–670. [[CrossRef](#)]
18. Fang, X.; Chen, Y.; Zhang, H.; Chen, W.; Dong, A.; Wang, R. Heat transfer and critical heat flux of nanofluid boiling: A comprehensive review. *Renew. Sustain. Energy Rev.* **2016**, *62*, 924–940. [[CrossRef](#)]
19. Dadhich, M.; Prajapati, O.S. A brief review on factors affecting flow and pool boiling. *Renew. Sustain. Energy Rev.* **2019**, *112*, 607–625. [[CrossRef](#)]
20. Kamel, M.S.; Lezsovits, F.; Hussein, A.K. Experimental studies of flow boiling heat transfer by using nanofluids. *J. Therm. Anal. Calorim.* **2019**, *138*, 4019–4043. [[CrossRef](#)]
21. Barber, J.; Brutin, D.; Tadrist, L. A review on b.+oiling heat transfer enhancement with nanofluids. *Nanoscale Res. Lett.* **2011**, *6*, 280. [[CrossRef](#)]
22. Khan, K.S.; Kunz, R.; Kleijnen, J.; Antes, G. Five steps to conducting a systematic review. *J. R. Soc. Med.* **2003**, *96*, 118–121. [[CrossRef](#)] [[PubMed](#)]
23. Genco, F.; Genco, G. Thermal Hydraulic Modeling and Analysis of Fusion Reactors Plasma Facing Components Using Alumina Nanofluids. *J. Therm. Sci. Eng. Appl.* **2017**, *9*, 031003. [[CrossRef](#)]
24. Pan, B.; Wang, W.; Chu, D.; Mei, L.; Zhang, Q. Experimental investigation of hypervapotron heat transfer enhancement with alumina–water nanofluids. *Int. J. Heat Mass Transf.* **2016**, *98*, 738–745. [[CrossRef](#)]
25. Jiang, H.; Wang, W.; Chu, D.; Lu, W.; Shu, X.; Wu, Y. Compatibility of fusion reactor materials with flowing nanofluids. *Fusion Eng. Des.* **2017**, *125*, 391–395. [[CrossRef](#)]
26. You, S.M.; Kim, J.H.; Kim, K.H. Effect of nanoparticles on critical heat flux of water in pool boiling heat transfer. *Appl. Phys. Lett.* **2003**, *83*, 3374–3376. [[CrossRef](#)]
27. Shoghl, S.N. Experimental investigation on pool boiling heat transfer of ZnO, and CuO water-based nanofluids and effect of surfactant on heat transfer coefficient. *Int. Commun. Heat Mass Transf.* **2013**, *45*, 122–129. [[CrossRef](#)]
28. Amiri, A.; Shanbedi, M.; Amiri, H.; Heris, S.Z.; Kazi, S.N.; Chew, B.T.; Eshghi, H. Pool boiling heat transfer of CNT/water nanofluids. *Appl. Therm. Eng.* **2014**, *71*, 450–459. [[CrossRef](#)]
29. Huang, C.-K.; Lee, C.-W.; Wang, C.-K. Boiling enhancement by TiO₂ nanoparticle deposition. *Int. J. Heat Mass Transf.* **2011**, *54*, 4895–4903. [[CrossRef](#)]
30. Wen, D.; Corr, M.; Hu, X.; Lin, G. Boiling heat transfer of nanofluids: The effect of heating surface modification. *Int. J. Therm. Sci.* **2011**, *50*, 480–485. [[CrossRef](#)]
31. Harish, G.; Emlin, V.; Sajith, V. Effect of surface particle interactions during pool boiling of nanofluids. *Int. J. Therm. Sci.* **2011**, *50*, 2318–2327. [[CrossRef](#)]
32. Sheikhbahai, M.; Esfahany, M.N.; Etesami, N. Experimental investigation of pool boiling of Fe₃O₄/ethylene glycol–water nanofluid in electric field. *Int. J. Therm. Sci.* **2012**, *62*, 149–153. [[CrossRef](#)]
33. Kole, M.; Dey, T.K. Thermophysical and pool boiling characteristics of ZnO-ethylene glycol nanofluids. *Int. J. Therm. Sci.* **2012**, *62*, 61–70. [[CrossRef](#)]
34. Mourgues, A.; Hourtané, V.; Muller, T.; Caron-Charles, M. Boiling behaviors and critical heat flux on a horizontal and vertical plate in saturated pool boiling with and without ZnO nanofluid. *Int. J. Heat Mass Transf.* **2013**, *57*, 595–607. [[CrossRef](#)]
35. Sarafraz, M.M.; Hormozi, F. Nucleate pool boiling heat transfer characteristics of dilute Al₂O₃–ethyleneglycol nanofluids. *Int. Commun. Heat Mass Transf.* **2014**, *58*, 96–104. [[CrossRef](#)]
36. Shahmoradi, Z.; Etesami, N.; Esfahany, M.N. Pool boiling characteristics of nanofluid on flat plate based on heater surface analysis. *Int. Commun. Heat Mass Transf.* **2013**, *47*, 113–120. [[CrossRef](#)]
37. Vafaei, S. Nanofluid pool boiling heat transfer phenomenon. *Powder Technol.* **2015**, *277*, 181–192. [[CrossRef](#)]
38. Cieśliński, J.T.; Kaczmarczyk, T.Z. Pool Boiling of Water–Al₂O₃ and Water–Cu Nanofluids Outside Porous Coated Tubes. *Heat Transf. Eng.* **2015**, *36*, 553–563. [[CrossRef](#)]
39. Niu, G.; Li, J. Comparative studies of pool boiling heat transfer with nano-fluids on porous surface. *Heat Mass Transf.* **2015**, *51*, 1769–1777. [[CrossRef](#)]
40. Kamatchi, R.; Venkatachalapathy, S.; Nithya, C. Experimental investigation and mechanism of critical heat flux enhancement in pool boiling heat transfer with nanofluids. *Heat Mass Transf.* **2016**, *52*, 2357–2366. [[CrossRef](#)]
41. Sarafraz, M.M.; Hormozi, F.; Silakhori, M.; Peyghambarzadeh, S.M. On the fouling formation of functionalized and non-functionalized carbon nanotube nano-fluids under pool boiling condition. *Appl. Therm. Eng.* **2016**, *95*, 433–444. [[CrossRef](#)]
42. Sayahi, T.; Bahrami, M. Investigation on the Effect of Type and Size of Nanoparticles and Surfactant on Pool Boiling Heat Transfer of Nanofluids. *J. Heat Transf.* **2015**, *138*, 031502. [[CrossRef](#)]
43. Manetti, L.L.; Stephen, M.T.; Beck, P.A.; Cardoso, E.M. Evaluation of the heat transfer enhancement during pool boiling using low concentrations of Al₂O₃-water based nanofluid. *Exp. Therm. Fluid Sci.* **2017**, *87*, 191–200. [[CrossRef](#)]
44. Mukherjee, S.; Mishra, P.C.; Chaudhuri, P. Pool boiling performance of aqueous Al₂O₃ and TiO₂ nanofluids on a horizontally placed flat polished surface: An experimental investigation. *J. Therm. Anal. Calorim.* **2020**, *146*, 415–433. [[CrossRef](#)]
45. Salimpour, M.R.; Abdollahi, A.; Afrand, M. An experimental study on deposited surfaces due to nanofluid pool boiling: Comparison between rough and smooth surfaces. *Exp. Therm. Fluid Sci.* **2017**, *88*, 288–300. [[CrossRef](#)]

46. Li, Z.; Sarafraz, M.M.; Mazinani, A.; Hayat, T.; Alsulami, H.; Goodarzi, M. Pool boiling heat transfer to CuO-H₂O nanofluid on finned surfaces. *Int. J. Heat Mass Transf.* **2020**, *156*, 119780. [[CrossRef](#)]
47. Koulouloulias, K.; Sergis, A.; Hardalupas, Y.; Barrett, T.R. Visualisation of subcooled pool boiling in nanofluids. *Fusion Eng. Des.* **2019**, *146*, 153–156. [[CrossRef](#)]
48. Etedali, S.; Afrand, M.; Abdollahi, A. Effect of different surfactants on the pool boiling heat transfer of SiO₂/deionized water nanofluid on a copper surface. *Int. J. Therm. Sci.* **2019**, *145*, 105977. [[CrossRef](#)]
49. Li, K.; Li, X.D.; Tu, J.Y.; Wang, H.G. A mathematic model considering the effect of Brownian motion for subcooled nucleate pool boiling of dilute nanofluids. *Int. J. Heat Mass Transf.* **2015**, *84*, 46–53. [[CrossRef](#)]
50. Kamel, M.S.; Al-agma, M.S.; Lezsovits, F.; Mahian, O. Simulation of pool boiling of nanofluids by using Eulerian multiphase model. *J. Therm. Anal. Calorim.* **2019**, *142*, 493–505. [[CrossRef](#)]
51. Salehi, H.; Hormozi, F. Numerical study of silica-water based nanofluid nucleate pool boiling by two-phase Eulerian scheme. *Heat Mass Transf.* **2018**, *54*, 773–784. [[CrossRef](#)]
52. Balcilar, M.; Dalkilic, A.S.; Suriyawong, A.; Yiamsawas, T.; Wongwises, S. Investigation of pool boiling of nanofluids using artificial neural networks and correlation development techniques. *Int. Commun. Heat Mass Transf.* **2012**, *39*, 424–431. [[CrossRef](#)]
53. Ganapathy, H.; Sajith, V. Semi-analytical model for pool boiling of nanofluids. *Int. J. Heat Mass Transf.* **2013**, *57*, 32–47. [[CrossRef](#)]
54. Gobinath, N.; Venugopal, T.; Palani, K.; Samuel, A.A. Numerical modelling of thermophoresis in water-alumina nanofluid under pool boiling conditions. *Int. J. Therm. Sci.* **2018**, *129*, 1–13. [[CrossRef](#)]
55. Sarafraz, M.M.; Arya, H.; Saedi, M.; Ahmadi, D. Flow boiling heat transfer to MgO-therminol 66 heat transfer fluid: Experimental assessment and correlation development. *Appl. Therm. Eng.* **2018**, *138*, 552–562. [[CrossRef](#)]
56. Karimzadehkhoei, M.; Sezen, M.; Şendur, K.; Mengüç, M.P.; Koşar, A. Subcooled flow boiling heat transfer of γ -Al₂O₃/water nanofluids in horizontal microtubes and the effect of surface characteristics and nanoparticle deposition. *Appl. Therm. Eng.* **2017**, *127*, 536–546. [[CrossRef](#)]
57. Hashemi, M.; Noie, S.H. Study of flow boiling heat transfer characteristics of critical heat flux using carbon nanotubes and water nanofluid. *J. Therm. Anal. Calorim.* **2017**, *130*, 2199–2209. [[CrossRef](#)]
58. Choi, Y.J.; Kam, D.H.; Jeong, Y.H. Analysis of CHF enhancement by magnetite nanoparticle deposition in the subcooled flow boiling region. *Int. J. Heat Mass Transf.* **2017**, *109*, 1191–1199. [[CrossRef](#)]
59. Rajabnia, H.; Abedini, E.; Tahmasebi, A.; Behzadmehr, A. Experimental investigation of subcooled flow boiling of water/TiO₂ nanofluid in a horizontal tube. *Therm. Sci.* **2014**, *20*, 99–108. [[CrossRef](#)]
60. Paul, G.; Das, P.K.; Manna, I. Assessment of the process of boiling heat transfer during rewetting of a vertical tube bottom flooded by alumina nanofluid. *Int. J. Heat Mass Transf.* **2016**, *94*, 390–402. [[CrossRef](#)]
61. Zangeneh, A.; Vatani, A.; Fakhroean, Z.; Peyghambarzadeh, S.M. Experimental study of forced convection and subcooled flow boiling heat transfer in a vertical annulus using different novel functionalized ZnO nanoparticles. *Appl. Therm. Eng.* **2016**, *109*, 789–802. [[CrossRef](#)]
62. Sarafraz, M.M.; Hormozi, F.; Peyghambarzadeh, S.M.; Vaeli, N. Upward flow boiling to DI-water and CuO nanofluids inside the concentric annuli. *J. Appl. Fluid Mech.* **2015**, *8*, 651–659. [[CrossRef](#)]
63. Setoodeh, H.; Keshavarz, A.; Ghasemian, A.; Nasouhi, A. Subcooled flow boiling of alumina/water nanofluid in a channel with a hot spot: An experimental study. *Appl. Therm. Eng.* **2015**, *90*, 384–394. [[CrossRef](#)]
64. Sarafraz, M.M.; Hormozi, F. Comparatively experimental study on the boiling thermal performance of metal oxide and multi-walled carbon nanotube nanofluids. *Powder Technol.* **2016**, *287*, 412–430. [[CrossRef](#)]
65. Rana, K.B.; Rajvanshi, A.K.; Agrawal, G.D. A visualization study of flow boiling heat transfer with nanofluids. *J. Vis.* **2013**, *16*, 133–143. [[CrossRef](#)]
66. Lee, S.-W.; Park, S.-D.; Kang, S.-R.; Kim, S.-M.; Seo, H.; Lee, D.W.; Bang, I.C. Critical heat flux enhancement in flow boiling of Al₂O₃ and SiC nanofluids under low pressure and low flow conditions. *Nucl. Eng. Technol.* **2012**, *44*, 429–436. [[CrossRef](#)]
67. Vafaei, S.; Wen, D. Spreading of triple line and dynamics of bubble growth inside nanoparticle dispersions on top of a substrate plate. *J. Colloid Interface Sci.* **2011**, *362*, 285–291. [[CrossRef](#)] [[PubMed](#)]
68. Vafaei, S.; Wen, D. Flow boiling heat transfer of alumina nanofluids in single microchannels and the roles of nanoparticles. *J. Nanopart. Res.* **2011**, *13*, 1063–1073. [[CrossRef](#)]
69. Lee, J.; Mudawar, I. Assessment of the effectiveness of nanofluids for single-phase and two-phase heat transfer in micro-channels. *Int. J. Heat Mass Transf.* **2007**, *50*, 452–463. [[CrossRef](#)]
70. Balasubramanian, K.R.; Krishnan, A.; Sivan, S. Transient Flow Boiling Performance and Critical Heat Flux Evaluation of Al₂O₃-Water Nanofluid in Parallel Microchannels. *J. Nanofluids* **2018**, *7*, 1035–1044. [[CrossRef](#)]
71. Abedini, E.; Zarei, T.; Afrand, M.; Wongwises, S. Experimental study of transition flow from single phase to two phase flow boiling in nanofluids. *J. Mol. Liq.* **2017**, *231*, 11–19. [[CrossRef](#)]
72. Patra, N.; Gupta, V.; Pradyumna, E.; Singh, R.; Ghosh, P.; Singh, R.S.; Nayak, A. Delay in DNB for flow boiling of diluted oxide based nanofluids. *Exp. Therm. Fluid Sci.* **2017**, *89*, 211–218. [[CrossRef](#)]
73. Zhang, C.; Zhang, L.; Xu, H.; Wang, D.; Ye, B. Investigation of flow boiling performance and the resulting surface deposition of graphene oxide nanofluid in microchannels. *Exp. Therm. Fluid Sci.* **2017**, *86*, 1–10. [[CrossRef](#)]
74. Zhang, S.Y.; Ge, Z.; Wang, H.T.; Wang, H. Characteristics of Flow Boiling Heat Transfer and Pressure Drop of MWCNT-R123 Nanorefrigerant: Experimental Investigations and Correlations. *Nanoscale Microscale Thermophys. Eng.* **2016**, *20*, 97–120. [[CrossRef](#)]

75. Tazarv, S.; Saffar-Avval, M.; Khalvati, F.; Mirzaee, E.; Mansoori, Z. Experimental Investigation of Saturated Flow Boiling Heat Transfer to TiO₂/R141b Nanorefrigerant. *Exp. Heat Transf.* **2016**, *29*, 188–204. [[CrossRef](#)]
76. Wang, Y.; Su, G.H. Experimental investigation on nanofluid flow boiling heat transfer in a vertical tube under different pressure conditions. *Exp. Therm. Fluid Sci.* **2016**, *77*, 116–123. [[CrossRef](#)]
77. Salari, E.; Sarafraz, M.; Peyghambarzadeh, S.M.; Hormozi, F. Boiling Heat Transfer of Alumina Nano-Fluids: Role of Nanoparticle Deposition on the Boiling Heat Transfer Coefficient. *Period. Polytech. Chem. Eng.* **2016**, *60*, 252–258. [[CrossRef](#)]
78. Soleimani, B.; Keshavarz, A. Heat transfer enhancement of an internal subcooled flow boiling over a hot spot. *Appl. Therm. Eng.* **2016**, *99*, 206–213. [[CrossRef](#)]
79. Moreira, T.A.; Nascimento, F.J.D.; Ribatski, G. An investigation of the effect of nanoparticle composition and dimension on the heat transfer coefficient during flow boiling of aqueous nanofluids in small diameter channels (1.1 mm). *Exp. Therm. Fluid Sci.* **2017**, *89*, 72–89. [[CrossRef](#)]
80. Lee, J.H.; Lee, T.; Jeong, Y.H. The effect of pressure on the critical heat flux in water-based nanofluids containing Al₂O₃ and Fe₃O₄ nanoparticles. *Int. J. Heat Mass Transf.* **2013**, *61*, 432–438. [[CrossRef](#)]
81. Xu, L.; Xu, J. Nanofluid stabilizes and enhances convective boiling heat transfer in a single microchannel. *Int. J. Heat Mass Transf.* **2012**, *55*, 5673–5686. [[CrossRef](#)]
82. Wang, Y.; Deng, K.; Wu, J.; Su, G.; Qiu, S. The characteristics and correlation of nanofluid flow boiling critical heat flux. *Int. J. Heat Mass Transf.* **2018**, *122*, 212–221. [[CrossRef](#)]
83. Rabiee, A.; Atf, A. Simulation of nanofluid dryout phenomenon in a PWR rod bundle with mixing vanes using computational fluid dynamics. *Prog. Nucl. Energy* **2018**, *109*, 270–279. [[CrossRef](#)]
84. Abedini, E.; Zarei, T.; Rajabnia, H.; Kalbasi, R.; Afrand, M. Numerical investigation of vapor volume fraction in subcooled flow boiling of a nanofluid. *J. Mol. Liq.* **2017**, *238*, 281–289. [[CrossRef](#)]
85. Esfe, M.H. Designing a neural network for predicting the heat transfer and pressure drop characteristics of Ag/water nanofluids in a heat exchanger. *Appl. Therm. Eng.* **2017**, *126*, 559–565. [[CrossRef](#)]
86. Wang, Y.; Deng, K.H.; Liu, B.; Wu, J.M.; Su, G.H. A correlation of nanofluid flow boiling heat transfer based on the experimental results of AlN/H₂O and Al₂O₃/H₂O nanofluid. *Exp. Therm. Fluid Sci.* **2017**, *80*, 376–383. [[CrossRef](#)]
87. Rakhsha, M.; Akbaridoust, F.; Abbassi, A.; Majid, S.-A. Experimental and numerical investigations of turbulent forced convection flow of nano-fluid in helical coiled tubes at constant surface temperature. *Powder Technol.* **2015**, *283*, 178–189. [[CrossRef](#)]
88. Aminfar, H.; Mohammadpourfard, M.; Maroofiazar, R. Numerical study of non-uniform magnetic fields effects on subcooled nanofluid flow boiling. *Prog. Nucl. Energy* **2014**, *74*, 232–241. [[CrossRef](#)]
89. Sasmito, A.P.; Kurnia, J.C.; Mujumdar, A.S. Numerical evaluation of laminar heat transfer enhancement in nanofluid flow in coiled square tubes. *Nanoscale Res. Lett.* **2011**, *6*, 376. [[CrossRef](#)] [[PubMed](#)]
90. Purbia, D.; Khandelwal, A.; Kumar, A.; Sharma, A.K. Graphene-water nanofluid in heat exchanger: Mathematical modelling, simulation and economic evaluation. *Int. Commun. Heat Mass Transf.* **2019**, *108*, 104327. [[CrossRef](#)]
91. Tafarroj, M.M.; Mahian, O.; Kasaeian, A.; Sakamatapan, K.; Dalkilic, A.S.; Wongwises, S. Artificial neural network modeling of nanofluid flow in a microchannel heat sink using experimental data. *Int. Commun. Heat Mass Transf.* **2017**, *86*, 25–31. [[CrossRef](#)]
92. Mohammadpourfard, M.; Aminfar, H.; Karimi, M. Numerical investigation of non-uniform transverse magnetic field effects on the swirling flow boiling of magnetic nanofluid in annuli. *Int. Commun. Heat Mass Transf.* **2016**, *75*, 240–252. [[CrossRef](#)]